

AD-A061 804

MCDONNELL DOUGLAS RESEARCH LABS ST LOUIS MO
INFLUENCE OF RARE-EARTH ADDITIONS ON PROPERTIES OF TITANIUM ALL--ETC(U)
MAY 78 C R WHITSETT, S M SASTRY, J E O'NEAL N00014-76-C-0626
MDC-Q0654 NL

UNCLASSIFIED

| OF |
AD
A061804



END
DATE
FILMED
2 79
DDC

AD A061804

INFLUENCE OF RARE-EARTH ADDITIONS ON PROPERTIES OF TITANIUM ALLOYS

12
5c

Room-Temperature Tensile Properties and Fracture Toughness of Ti-6Al-4V with Erbium, Yttrium, and Vanadium Additions

C.R. Whitsett, S.M.L. Sastry, J.E. O'Neil, and R.L. Campbell

McDonnell Douglas Research Laboratories
St. Louis, Missouri 63166

31 May 1978

Technical Report for period 1 April 1977 - 31 March 1978

Approved for public release; distribution unlimited

Prepared for:
DEPARTMENT OF THE NAVY
Office of Naval Research
800 S. Galaxy Street
Arlington, VA 22217

DDC
POPULAR
DEC 4 1978
F

DDC FILE COPY

MCDONNELL DOUGLAS RESEARCH LABORATORIES

MCDONNELL DOUGLAS



CORPORATION

78 11 30 035

UNCLASSIFIED

SECURITY CLASSIFICATION OF THIS PAGE (When Data Entered)

REPORT DOCUMENTATION PAGE		READ INSTRUCTIONS BEFORE COMPLETING FORM
1. REPORT NUMBER	2. GOVT ACCESSION NO.	3. RECIPIENT'S CATALOG NUMBER
6. TITLE (and Subtitle) INFLUENCE OF RARE-EARTH ADDITIONS ON PROPERTIES OF TITANIUM ALLOYS. Room-Temperature Tensile Properties and Fracture Toughness of Ti-6Al-4V with Erbium, Yttrium, and Yttria Additions.		5. TYPE OF REPORT & PERIOD COVERED Technical Report 1 April 1977-31 March 1978.
7. AUTHOR(s) C. R. Whitsett, S. M. L. Sastry, J. E. O'Neal and R. J. Lederich		6. PERFORMING ORG. REPORT NUMBER 14 MDC-Q0654
9. PERFORMING ORGANIZATION NAME AND ADDRESS McDonnell Douglas Research Laboratories McDonnell Douglas Corporation St. Louis, Missouri 63166		8. CONTRACT OR GRANT NUMBER(s) N00014-76-C-0626
11. CONTROLLING OFFICE NAME AND ADDRESS Office of Naval Research 800 N. Quincy Street Arlington, Virginia 22217		10. PROGRAM ELEMENT, PROJECT, TASK AREA & WORK UNIT NUMBERS
14. MONITORING AGENCY NAME & ADDRESS (if different from Controlling Office)		12. REPORT DATE 11 31 May 1978
		13. NUMBER OF PAGES 67 12 68p
		15. SECURITY CLASS. (of this report) Unclassified
		15a. DECLASSIFICATION/DOWNGRADING SCHEDULE
16. DISTRIBUTION STATEMENT (of this Report) Approved for public release; distribution unlimited.		
17. DISTRIBUTION STATEMENT (of the abstract entered in Block 20, if different from Report)		
18. SUPPLEMENTARY NOTES		
19. KEY WORDS (Continue on reverse side if necessary and identify by block number) Titanium alloy Microstructure Elongation Ti-6Al-4V Grain refinement Ductility Yttrium Second-phase dispersion Fracture toughness Erbium Yield stress Texture Yttria Ultimate tensile stress		
20. ABSTRACT (Continue on reverse side if necessary and identify by block number) The influence of additions of 0.1 wt% Er, 0.02 wt% Y, 0.05 wt% Y, and 0.038 wt% Y ₂ O ₃ on the room-temperature tensile properties and fracture toughness of Ti-6Al-4V was studied. The alloys were cast by consumable-electrode arc-melting in vacuum. Er and Y were added in the form of Ti-25Er and Ti-25Y master alloys, and Y ₂ O ₃ was added in the form of a fine powder. The alloys, after being forged and rolled, had only about half the nominal concentrations of rare-earth additives. The rolled plates were given various heat treatments		

405 315

UNCLASSIFIED

SECURITY CLASSIFICATION OF THIS PAGE(When Data Entered)

to observe the combined effects of microstructure and rare-earth additives. The rare-earths effect grain refinement. The room-temperature tensile properties and fracture toughness of Ti-6Al-4V are not significantly altered by the rare-earths. The crystallographic texture developed during rolling also is unaffected by the rare-earth additives, although Y and Y_2O_3 effect an increased sharpness of near-transverse-basal texture components in α - β annealed alloy. The uniform elongation of Ti-6Al-4V under tensile stress at high temperatures is increased by Er and Y additions. The high-temperature compressive stress-strain characteristics of heat treated Ti-6Al-4V are not altered by Er and Y.

alpha-beta

ACCESSION for	
NTIS	White Section <input checked="" type="checkbox"/>
DDC	Buff Section <input type="checkbox"/>
UNANNOUNCED	
JUSTIFICATION	
BY DISTRIBUTION AVAILABILITY CODES	
Dist.	SPECIAL
A	

UNCLASSIFIED

SECURITY CLASSIFICATION OF THIS PAGE(When Data Entered)

PREFACE

This report presents the results of the second phase of an investigation of the effects of rare-earth additives on titanium alloys performed by the McDonnell Douglas Research Laboratories under Office of Naval Research Contract No. N00014-76-C-0626. The scientific officer for the contract is Dr. Bruce A. MacDonald of ONR.

The principal investigator is Dr. Charles R. Whitsett. Co-investigators are Dr. Shankar M. L. Sastry, Mr. James E. O'Neal and Mr. Richard J. Lederich. The cooperation and attention to detail of Dr. F. H. Froes, Mr. V. C. Peterson, and Mr. C. F. Yolton of the Crucible Materials Research Center in the preparation of alloys for this study are gratefully acknowledged.

This report has been reviewed and is approved.

C. R. Whitsett

Charles R. Whitsett
Chief Scientist - Solid State Sciences
McDonnell Douglas Research Laboratories

D. P. Ames

Donald P. Ames
Staff Vice President
McDonnell Douglas Research Laboratories

Bruce A. MacDonald
Bruce A. MacDonald
Office of Naval Research

TABLE OF CONTENTS

	<u>Page</u>
1 INTRODUCTION	1
2 ALLOY PREPARATIONS	2
2.1 Ingot Melting, Forging and Rolling of Phase II Ti-6Al-4V-RE Alloys	2
2.2 Chemical Analyses of the Alloys	4
2.3 Heat Treatment of the Alloys	6
3 MICROSTRUCTURAL CHARACTERIZATION	7
4 CRYSTALLOGRAPHIC TEXTURE	13
5 ROOM-TEMPERATURE TENSILE PROPERTIES	19
6 FRACTURE TOUGHNESS	25
7 PLANE-STRESS FRACTURE TOUGHNESS	29
8 HIGH-TEMPERATURE DEFORMATION OF PHASE-II Ti-6Al-4V-RE ALLOYS	34
8.1 High-Temperature Tensile Tests	34
8.2 High-Temperature Compression Test	37
8.3 High-Temperature Deformation Substructures	43
9 CONCLUSIONS	47
REFERENCES	48
APPENDIX A	49
DISTRIBUTION	55

PRECEDING PAGE BLANK

LIST OF ILLUSTRATIONS

Figure		Page
1	Microstructures of Ti-RE master alloys: (a) Ti-25Er and (b) Ti-25Y	3
2	Rolling schedule for Phase-II Ti-6Al-4V-RE alloys	4
3	Microstructures of alloys processed per schedule A; (a) Ti-6Al-4V reference alloy, (b) Ti-6Al-4V-0.1Er, (c) Ti-6Al-4V-0.05Y, and (d) Ti-6Al-4V-0.038Y ₂ O ₃	8
4	Microstructures of alloys processed per schedule B; (a) Ti-6Al-4V reference alloy, (b) Ti-6Al-4V-0.1Er, (c) Ti-6Al-4V-0.05Y, and (d) Ti-6Al-4V-0.038Y ₂ O ₃	9
5	Transmission electron micrographs of alloys processed per schedule A; (a) Ti-6Al-4V reference alloy, (b) Ti-6Al-4V-0.10Er, (c) Ti-6Al-4V-0.05Y, and (d) Ti-6Al-4V-0.038Y ₂ O ₃	10
6	Microstructures of beta-annealed Ti-6Al-4V-RE alloys; (a) Ti-6Al-4V reference alloy, (b) Ti-6Al-4V-0.1Er, (c) Ti-6Al-4V-0.05Y, and (d) Ti-6Al-4V-0.038Y ₂ O ₃	11
7	Microstructures of (a) Ti-6Al-4V reference alloy and (b) Ti-6Al-4V-0.02Y alloy processed per schedule B and recrystallization annealed	12
8	Texture development in alloys processed per schedule A; (a) Ti-6Al-4V reference alloy, (b) Ti-6Al-4V-0.1Er, (c) Ti-6Al-4V-0.05Y, and (d) Ti-6Al-4V-0.038Y ₂ O ₃ : (0002) pole figures are shown	14
9	Effects of beta annealing on texture of Ti-6Al-4V-RE alloys; (a) Ti-6Al-4V reference alloy, (b) Ti-6Al-4V-0.1Er, (c) Ti-6Al-4V-0.05Y, and (d) Ti-6Al-4V-0.038Y ₂ O ₃ : (0002) pole figures shown	15
10	Effect of recrystallization annealing on texture of Ti-6Al-4V-RE alloys; (a) Ti-6Al-4V reference alloy, (b) Ti-6Al-4V-0.1Er, (c) Ti-6Al-4V-0.05Y, and (d) Ti-6Al-4V-0.038Y ₂ O ₃ : (0002) pole figures are shown	16
11	Effect of solution-treatment-and-overaging on texture of Ti-6Al-4V-RE alloys; (a) Ti-6Al-4V reference alloy, (b) Ti-6Al-4V-0.1Er, (c) Ti-6Al-4V-0.05Y, and (d) Ti-6Al-4V-0.038Y ₂ O ₃ : (0002) pole figures are shown	17

LIST OF ILLUSTRATIONS (continued)

Figure		Page
12	Texture development in alloys processed per schedule B; (a) Ti-6Al-4V-0.05Y and (b) Ti-6Al-4V-0.038Y ₂ O ₃ : (10 $\bar{1}$ 0) pole figures are shown	18
13	Effect of recrystallization annealing on texture of alloys processed as per schedule B; (a) Ti-6Al-4V-0.05Y and (b) Ti-6Al-4V-0.038Y ₂ O ₃ : (10 $\bar{1}$ 0) pole figures are shown	18
14	Yield stress of hot-rolled and unannealed Ti-6Al-4V-RE alloys . .	20
15	Yield stress of beta-annealed Ti-6Al-4V-RE alloys	20
16	Yield stress of recrystallization annealed Ti-6Al-4V-RE alloys .	21
17	Yield stress of solution-treat-and-overaged Ti-6Al-4V-RE alloys .	21
18	Yield stress of α - β annealed and aged Ti-6Al-4V-RE alloys	22
19	Total elongation of hot-rolled and unannealed Ti-6Al-4V-RE alloys	22
20	Total elongation of beta-annealed Ti-6Al-4V-RE alloys	23
21	Total elongation of recrystallization annealed Ti-6Al-4V-RE alloys	23
22	Total elongation of solution-treat-and-overaged Ti-6Al-4V-RE alloys	24
23	Total elongation of α - β annealed and aged Ti-6Al-4V-RE alloys . .	24
24	Fracture toughness (K_Q) of beta-annealed Ti-6Al-4V-RE alloys processed according to schedule B	26
25	Fracture toughness (K_Q) of beta-annealed Ti-6Al-4V-RE alloys processed according to schedule A	26
26	Fracture toughness (K_Q) of recrystallization-annealed Ti-6Al-4V-RE Alloys processed according to schedule B	27
27	Fracture toughness (K_Q) of recrystallization-annealed Ti-6Al-4V-RE alloys processed according to schedule A	27
28	Fracture toughness (K_Q) of solution-treat-and-overaged Ti-6Al- 4V-RE alloys processed according to schedule B	28
29	Fracture toughness (K_Q) of solution-treat-and-overaged Ti-6Al-4V- RE alloy processed according to schedule A	28
30	Specimen geometry and mounting of crack-opening-displacement gauge for measurement of plane-stress fracture-toughness	30

LIST OF ILLUSTRATIONS (continued)

Figure		Page
31	Schematic representation of plane-stress fracture-toughness determination	31
32	Plane-stress fracture toughness of beta-annealed Ti-6Al-4V-RE alloys	32
33	Plane-stress fracture toughness of recrystallization-annealed Ti-6Al-4V-RE alloys processed according to schedule A	32
34	Plane-stress fracture toughness of solution-treat-and-overaged Ti-6Al-4V-RE alloys	33
35	Photographs of two sets of Ti-6Al-4V-RE alloys processed per schedule B and deformed 40% in tension at 870°C at a strain rate of 0.1 s^{-1}	35
36	Details of α - β microstructure observed in Ti-6Al-4V specimens deformed at 800°C at a strain rate of 0.1 s^{-1} ; (a) bright-field electron micrograph, (b) selected-area diffraction pattern, (c) dark-field electron micrograph with α reflection, and (d) dark-field electron micrograph of the interface phase	36
37	Effects of temperature and strain-rate on deformation substructure of Ti-6Al-4V specimens deformed in tension; (a) undeformed, (b) $T = 800^\circ\text{C}$, $\dot{\epsilon} = 0.01 \text{ s}^{-1}$, (c) $T = 800^\circ\text{C}$, $\dot{\epsilon} = 0.1 \text{ s}^{-1}$, and (d) $T = 856^\circ\text{C}$, $\dot{\epsilon} = 0.01 \text{ s}^{-1}$	37
38	True-stress as a function of true-strain for beta-annealed Ti-6Al-4V-RE alloys deformed at 700°C at an initial strain rate of 0.05 s^{-1}	38
39	True-stress as a function of true-strain for beta-annealed Ti-6Al-4V-RE alloys deformed at 850°C at an initial strain-rate of 0.05 s^{-1}	39
40	True-stress as a function of true-strain for beta-annealed Ti-6Al-4V-RE alloys deformed at 900°C at an initial strain rate of 0.05 s^{-1}	40
41	True-stress as a function of true-strain for mill-annealed Ti-6Al-4V-RE alloys deformed at 700°C at an initial strain rate of 0.05 s^{-1}	41
42	True-stress as a function of true-strain for mill-annealed Ti-6Al-4V-RE alloys deformed at 800°C at an initial strain rate	

LIST OF ILLUSTRATIONS (continued)

Figure	Page
of 0.05 s^{-1}	42
43 True-stress as a function of true-strain for mill-annealed Ti-6Al-4V-RE alloys deformed at 850°C at an initial strain rate of 0.05 s^{-1}	42
44 Effect of temperature on deformation substructures of beta- annealed Ti-6Al-4V specimens deformed in compression at an initial strain rate of 0.05 s^{-1} ; (a) 700°C , (b) 800°C , (c) 850°C , and (d) 900°C	43
45 Effect of strain rate on deformation substructure of beta-annealed Ti-6Al-4V specimens deformed in compression at 700°C ; (a) strain rate = 0.001 s^{-1} and (b) strain rate = 0.05 s^{-1}	44
46 Effect of temperature on the deformation substructure of mill- annealed Ti-6Al-4V specimens deformed in compression at an initial strain rate of 0.05 s^{-1} ; (a) 700°C , (b) 800°C , and (c) 850°C . .	46

LIST OF TABLES

Table		Page
1	CHEMICAL ANALYSES OF PHASE-II Ti-6Al-4V-RE ALLOYS PERFORMED BY CRUCIBLE MATERIALS RESEARCH CENTER	5
2	CHEMICAL ANALYSES OF PHASE-II Ti-6Al-4V-RE ALLOYS PERFORMED BY UNITED STATES TESTING COMPANY, INC.	6
3	HEAT TREATMENT SCHEDULES FOR PHASE-II Ti-6Al-4V-RE ALLOYS	6
A1	ROOM-TEMPERATURE TENSILE PROPERTIES OF PHASE-II Ti-6Al-4V-RE ALLOYS IN THE LONGITUDINAL (L) AND TRANSVERSE (T) DIRECTIONS; HOT-ROLLED AND UNANNEALED, AS RECEIVED	49
A2	ROOM-TEMPERATURE TENSILE PROPERTIES OF PHASE-II Ti-6Al-4V-RE ALLOYS IN THE LONGITUDINAL (L) AND TRANSVERSE (T) DIRECTIONS: RECRYSTALLIZATION ANNEALED	50
A3	ROOM-TEMPERATURE TENSILE PROPERTIES OF PHASE-II Ti-6Al-4V-RE ALLOYS IN THE LONGITUDINAL (L) AND TRANSVERSE (T) DIRECTIONS; BETA ANNEALED	50
A4	ROOM-TEMPERATURE TENSILE PROPERTIES OF PHASE-II Ti-6Al-4V-RE ALLOYS IN THE LONGITUDINAL (L) AND TRANSVERSE (T) DIRECTIONS; SOLUTION-TREAT-AND-AGED	51
A5	ROOM-TEMPERATURE TENSILE PROPERTIES OF PHASE-II Ti-6Al-4V-RE ALLOYS IN THE LONGITUDINAL (L) AND TRANSVERSE (T) DIRECTIONS; SOLUTION-TREAT-AND-OVERAGED	51
A6	ROOM-TEMPERATURE TENSILE PROPERTIES OF PHASE-II Ti-6Al-4V-RE ALLOYS IN THE LONGITUDINAL (L) AND TRANSVERSE (T) DIRECTIONS: α - β ANNEALED AND AGED	52
A7	FRACTURE TOUGHNESS VALUES (K_Q) DETERMINED FROM SLOW-BEND, PRECRACKED, CHARPY SAMPLES OF RECRYSTALLIZATION-ANNEALED PHASE-II Ti-6Al-4V-RE ALLOYS	52
A8	FRACTURE TOUGHNESS VALUES (K_Q) DETERMINED FROM SLOW-BEND, PRECRACKED, CHARPY SAMPLES OF BETA-ANNEALED PHASE-II Ti-6Al-4V-RE ALLOYS	53
A9	FRACTURE TOUGHNESS VALUES (K_Q) DETERMINED FROM SLOW-BEND PRECRACKED, CHARPY SAMPLES OF SOLUTION-TREAT-AND-OVERAGED PHASE-II Ti-6Al-4V-RE ALLOYS	53
A10	PLANE-STRESS FRACTURE TOUGHNESS VALUES DETERMINED FROM CENTER-CRACKED TENSION SPECIMENS OF PHASE-II Ti-6Al-4V-RE ALLOYS	54

1. INTRODUCTION

A systematic investigation is being conducted of the effects of rare-earth (RE) additions to Ti-6Al-4V. In the first phase of this investigation¹ the influence of different concentrations of erbium, yttrium, and mischmetal on the microstructure and room-temperature tensile properties of Ti-6Al-4V subjected to various annealing procedures was determined. In Phase I, 0.1 wt% Er and 0.02-0.05 wt% Y in Ti-6Al-4V were determined to be effective for grain refinement and to not adversely affect the room-temperature tensile properties. In Phase II, which is reported here, Ti-6Al-4V with these Er and Y concentrations was more intensively characterized with respect to effects of different annealing procedures on room-temperature tensile and fracture-toughness characteristics and crystallographic texture development. For direct comparison of the effects of Y_2O_3 , one ingot with 0.038 wt% Y_2O_3 was prepared with the same alloy chemistry as the Er- and Y-modified Ti-6Al-4V. Phase III alloys have been prepared for plane-strain fracture toughness, creep, and high-temperature deformation studies, and these results will be presented in a subsequent report.

A recent study² showed that Y_2O_3 -additive is a beta-grain refiner in Ti-6Al-4V and significantly improves ingot forgeability. When Y_2O_3 powder is added to Ti-6Al-4V, it remains as large (1-10 μm) inclusions, which tend to agglomerate in Ti-6Al-4V and can degrade the tensile strength and fracture toughness, particularly in the short-transverse direction. Previous studies³⁻⁵ of rare-earth additives to α -Ti showed that metallic Y and Er dissolve in the molten Ti and precipitate as fine and uniformly-distributed particles, which effectively refine the microstructure of Ti. A near-term objective of this research is to demonstrate that a uniform, fine dispersion of metallic rare-earth additives in Ti-6Al-4V can improve the high-temperature formability, and thus reduce fabrication costs, of the alloy without adversely affecting strength and toughness.

The results presented in this report show that the room-temperature tensile properties and plane-strain and plane-stress fracture-toughness of Ti-6Al-4V are not adversely affected by 0.10 wt% Er and 0.02-0.05 wt% Y additions. The effects of Y_2O_3 additive on the properties of Ti-6Al-4V are qualitatively similar to but less pronounced than the effects of metallic-Y additive.

2. ALLOY PREPARATIONS*

2.1 Ingot Melting, Forging and Rolling of Phase II Ti-6Al-4V-RE Alloys

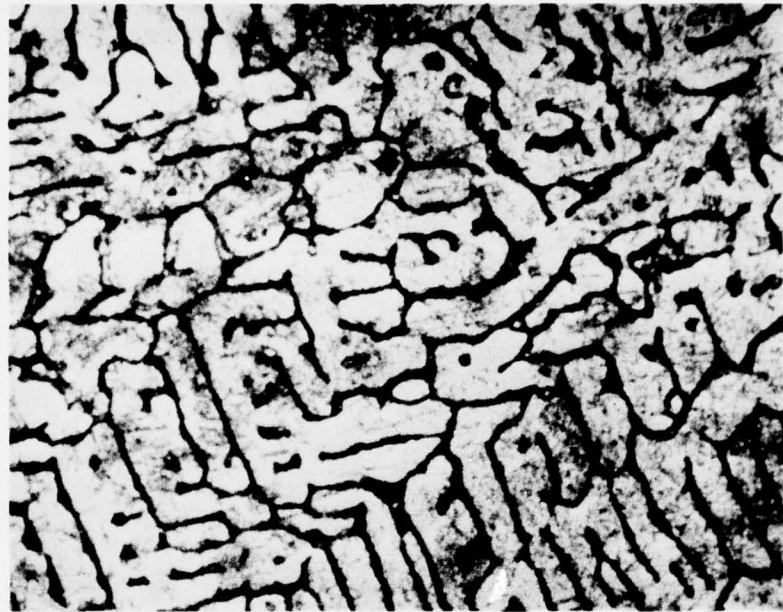
Five 14-kg ingots were cast with the nominal compositions Ti-6Al-4V, Ti-6Al-4V-0.10Er, Ti-6Al-4V-0.020Y, Ti-6Al-4V-0.050Y, and Ti-6Al-4V-0.038Y₂O₃. The alloy with 0.038 wt% Y₂O₃ was prepared to obtain data for directly comparing the relative effects of adding Y in the metallic and oxide forms. The same raw materials were used for the Phase II alloys as for Phase I. The charge for each alloy was blended and pressed into twelve 76-mm diam briquettes. The Ti-RE master alloy was broken into small pieces, wrapped in Ti foil, and inserted between the briquettes, which were then welded together to form a single-pole electrode. In the case of Y₂O₃ additive, the Y₂O₃ powder was tumbled with the Ti-sponge used to make the briquettes. The electrode was consumably melted into a 100-mm diam, water-cooled, copper mold, and the resultant ingot was inverted and remelted into a 143-mm diam, water-cooled, copper mold.

For the earlier, Phase-I alloys, the rare-earths were added to the consumable electrodes either in the elemental form or as 75Al-25RE master alloys. The Al-RE master alloys had undesired inclusions, and therefore for the Phase-II alloys, 75Ti-25RE master alloys were used. The Ti-RE master alloys, which were prepared at the Naval Research Laboratories by levitation melting in vacuum, had the hypoeutectic microstructures shown in Figure 1 and showed no evidence of inclusions or oxidation of the rare-earths.

Each ingot was coated with Metlseal RA-537[†] to minimize oxidation during forging. The ingots were heated to 1095°C, upset-forged 30%, and drawn out to 136-mm width and thickness. The ingots were then reheated to 1095°C, drawn out to 114-mm width and thickness, again reheated to 1095°C, and drawn out to 114-mm width and 51-mm thickness. All ingots forged well with little cracking or void formation.

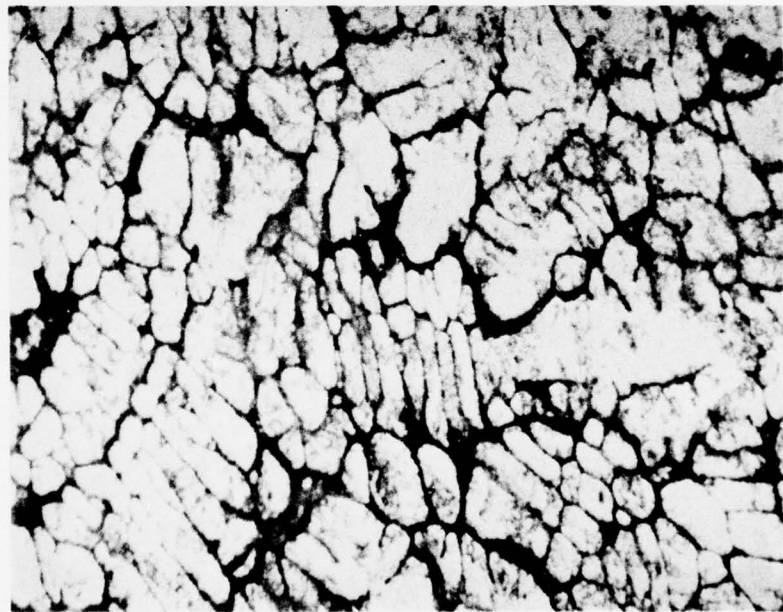
* Ingots for this investigation were cast, forged, and rolled by Crucible Materials Research Center, Colt Industries, Inc., Pittsburgh, PA.

[†] Tradename of Glidden-Durkee Division of SCM Corp., Cleveland, OH.



(a)

100 μm



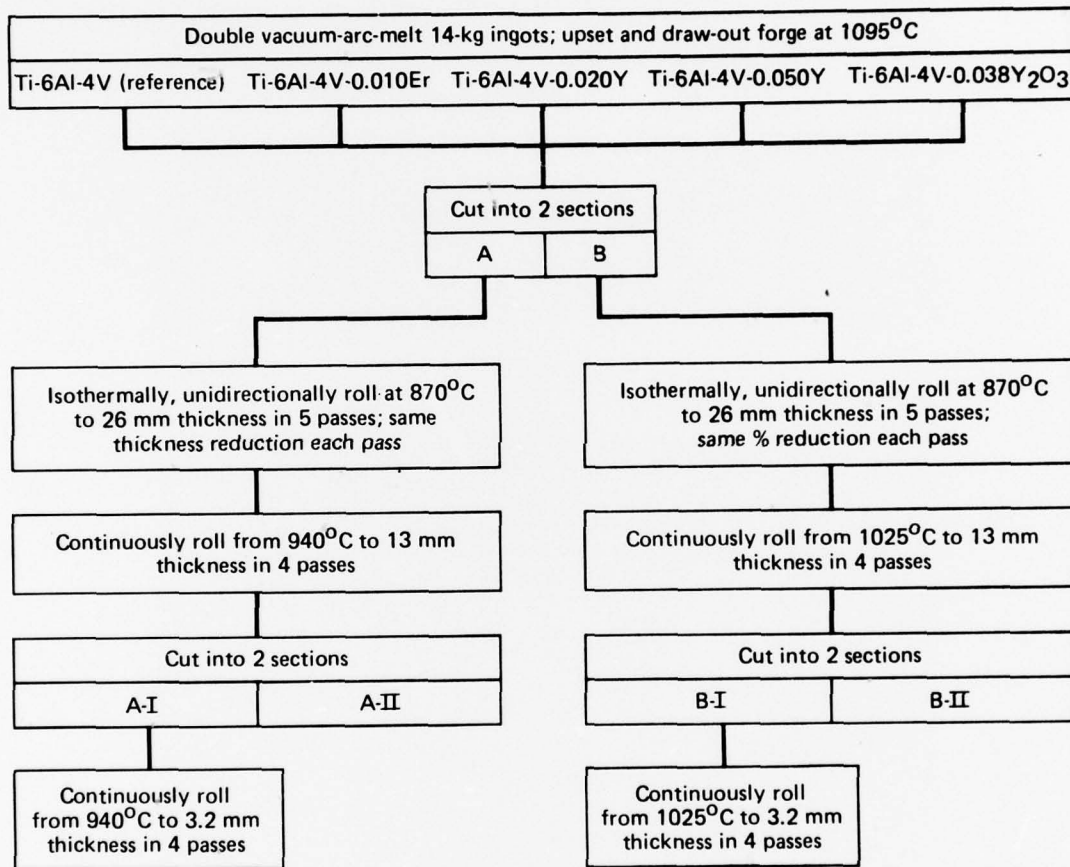
(b)

100 μm

GP78-0835-15

Figure 1. Microstructures of Ti-RE master alloys: (a) Ti-25Er and (b) Ti-25Y

The alloys were rolled according to the schedule shown in Figure 2. The different rolling schedules were designed to obtain qualitative hot-formability data in the form of rolling pressures required, but the plates were too small to obtain significant rolling-pressure data.



GP78-0635-16

Figure 2. Rolling schedule for Phase-II Ti-6Al-4V-RE alloys

2.2 Chemical Analyses of the Alloys

The chemical analyses performed by the Crucible Materials Research Center (CMRC) are summarized in Table 1. Samples for analysis were cut from the 13-mm thick plates and are representative of material at the mid-heights of the original ingots. The principal alloying elements and interstitial impurities are within the expected ranges. CMRC did not analyze for Er. The

Y concentration in the reference alloy is < 10 ppm. The alloys to which Y was added had 0.013 wt% and 0.052 wt% Y. The Y₂O₃-containing alloy has 0.012 wt% Y, which is about half the concentration corresponding to the addition of 0.038 wt% Y₂O₃ to the starting material.

TABLE 1. CHEMICAL ANALYSES OF PHASE-II Ti-6Al-4V-RE ALLOYS PERFORMED BY CRUCIBLE MATERIALS RESEARCH CENTER

Alloy code	Rare earth addition (wt%)	Chemical analysis (wt %)							
		Al	V	Fe	C	N	O	H	Y
31	None	6.0	4.1	0.08	0.028	0.016	0.118	0.0054	< 0.001
32	0.10Er	6.1	4.1	0.08	0.030	0.017	0.120	0.0067	—
33	0.020Y	6.1	4.1	0.06	0.026	0.016	0.125	0.0058	0.013
34	0.050Y	6.1	4.1	0.08	0.029	0.020	0.135	0.0060	0.052
36	0.038Y ₂ O ₃	6.1	4.1	0.08	0.026	0.016	0.126	0.0062	0.012

GP78-0635-2

Samples cut from different regions of the 13-mm and 3.2-mm plates were submitted for Er and Y analyses to the United States Testing Company (USTC)*, and the results are summarized in Table 2. The analyses were performed by x-ray fluorescence spectroscopy of the rare-earths precipitated as oxides in the case of USTC and precipitated as fluorides by CMRC. Measurements by CMRC on ten standards containing 0.0010 wt% Y gave an average concentration of 0.00075 wt% Y with a standard deviation of 0.00016 wt% Y, and measurements on ten standards containing 0.0040 wt% Y gave an average concentration of 0.0033 wt% Y with a standard deviation of 0.00056 wt%. The CMRC analytical method gives too low a value by up to 40%, although the method is reproducible to within ± 20%. USTC performed no analyses on standards, but they claim their method is accurate to within ± 5%.

The USTC analyses give Y and Er concentrations significantly lower than the nominal compositions and those reported by CMRC and indicate that the rare-earth concentration varies from region to region in a single alloy plate. Because of the analysis of errors on measurements of standards by CMRC, greater confidence may be placed on their Y determinations. It is probable that the rare-earth concentrations are approximately half the nominal concentrations used to describe the alloys in this report.

*United States Testing Company, Inc., 1415 Park Avenue, Hoboken, N. J. 07030.

2.3 Heat Treatment of the Alloys

The variously processed plates were heat treated according to the schedules shown in Table 3.

TABLE 2. CHEMICAL ANALYSES OF PHASE-II Ti-6Al-4V-RE ALLOYS PERFORMED BY UNITED STATES TESTING COMPANY, INC.

Alloy	Nominal composition	Specimen no.	Concentration of RE (wt%)
32	Ti-6Al-4V-0.10Er	1	0.059
		2	0.075
		3	0.061
		4	0.064
33	Ti-6Al-4V-0.02Y	1	< 0.0025
		2	< 0.0025
		3	0.004
		4	0.007
		5	0.0125
34	Ti-6Al-4V-0.05Y	1	0.005
		2	0.007
		3	0.022
36	Ti-6Al-4V-0.038Y ₂ O ₃	1	0.0025
		2	< 0.0025

GP78-0635-3

TABLE 3. HEAT TREATMENT SCHEDULES FOR PHASE-II Ti-6Al-4V-RE ALLOYS

Heat treatment	Schedule
Recrystallization anneal	930°C for 4 h; furnace-cool to 700°C; air-cool to 25°C
Beta anneal	1040°C for 0.5 h; air cool to 25°C; re-anneal at 700°C for 2 h; air-cool to 25°C
Solution treat and age	955°C for 2 h; water-quench; age at 550°C for 4 h; air-cool to 25°C
Solution treat and overage	955°C for 2 h; water-quench; age at 710°C for 4 h; air-cool to 25°C
α-β solution treat and age	955°C for 2 h; air-cool to 25°C; anneal at 710°C for 4 h; air-cool to 25°C

GP78-0635-4

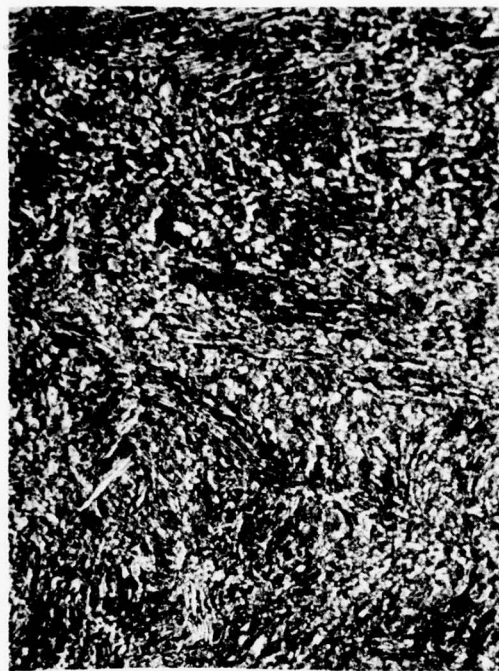
3. MICROSTRUCTURAL CHARACTERIZATION

The microstructures of the Phase-II reference alloy and rare-earth containing alloys processed according to schedules A and B are shown in Figures 3 and 4. The alloys processed per schedule A are characterized by a heavily-worked, unrecrystallized, two-phase microstructure. The Er and Y additions have no significant effect on the microstructure. Schedule B involved extensive rolling above the beta-transus temperature, which maintains a large volume-fraction of the β -phase during the rolling process. Consequently, the microstructure of the alloys processed according to schedule B consists of fine-scale transformed- β . The rare-earth-bearing alloys have a finer colony size than the reference alloy (Figure 4a-4c).

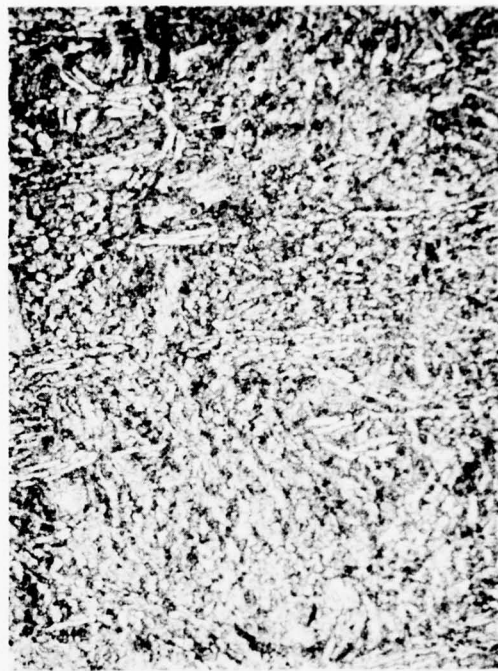
Figures 5a-5d are electron micrographs of the reference alloy and the rare-earth-containing alloys processed according to schedule A and subsequently recrystallization-annealed. The Er- and Y-bearing alloys contain small dispersoids in the size range 10-100 nm; however, the number of dispersoids in the thin foils was much lower than expected from the nominal rare-earth concentrations in the alloys.

The microstructures of the Phase-II alloys after the different heat treatments were as expected from the results for Phase-I alloys¹. The principal effect of the rare-earths is to reduce the colony and grain sizes of beta-annealed alloy, as is shown in Figures 6 and 7. There is no significant effect of the rare-earths on the microstructures of the alloys after recrystallization-annealing and solution-treat-and-aging. The alloys rolled per schedule B exhibit elongated alpha grains after recrystallization annealing (Figures 7a and 7b).

In addition to being given the conventional heat treatments as indicated in Table 3, the alloys were subjected to 1.0 h anneals at 600°, 700°, 800°, 900°, and 1000°C and water-quenched to determine their recrystallization behavior. The temperature for rapid recrystallization of the alloys is from 800° to 900°C. Whereas the alloys annealed at 800°C were only partially recrystallized, the alloys annealed at 900°C exhibited a completely recrystallized, two-phase microstructure consisting of grains of primary equiaxed-alpha and transformed-beta. The grain sizes in the alloys annealed at 900°C are 5-10 μm . The recrystallization temperature and the recrystallized $\alpha+\beta$ microstructure of Ti-6Al-4V are unaffected by the rare-earth additions.

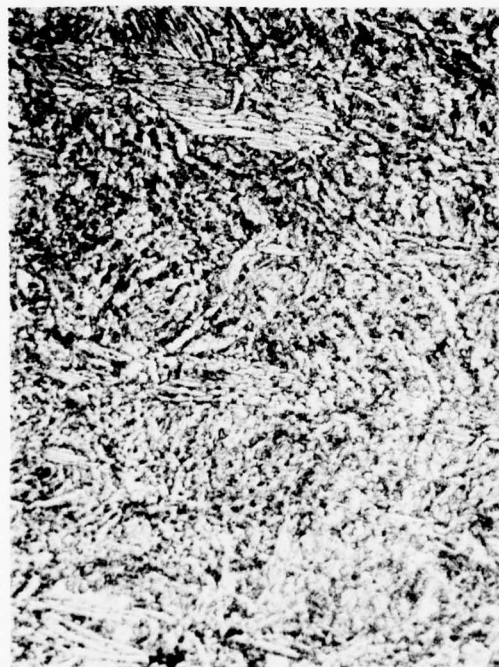


(a)

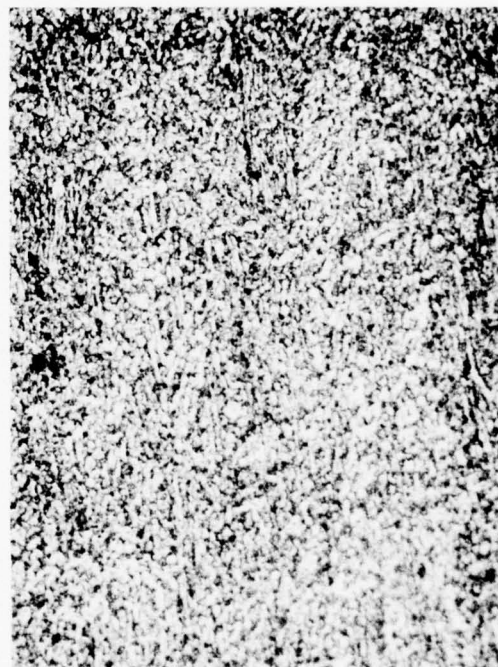


(b)

100 μm



(c)



(d)

100 μm

GP78-0635-17

Figure 3. Microstructures of alloys processed per schedule A: (a) Ti-6Al-4V reference alloy, (b) Ti-6Al-4V-0.10Er, (c) Ti-6Al-4V-0.05Y, and (d) Ti-6Al-4V-0.038Y₂O₃



(a)

100 μm



(b)



(c)

100 μm



(d)

GP78-0635-18

Figure 4. Microstructures of alloys processed per schedule B; (a) Ti-6Al-4V reference alloy, (b) Ti-6Al-4V-0.10Er, (c) Ti-6Al-4V-0.05Y, and (d) Ti-6Al-4V-0.038Y₂O₃

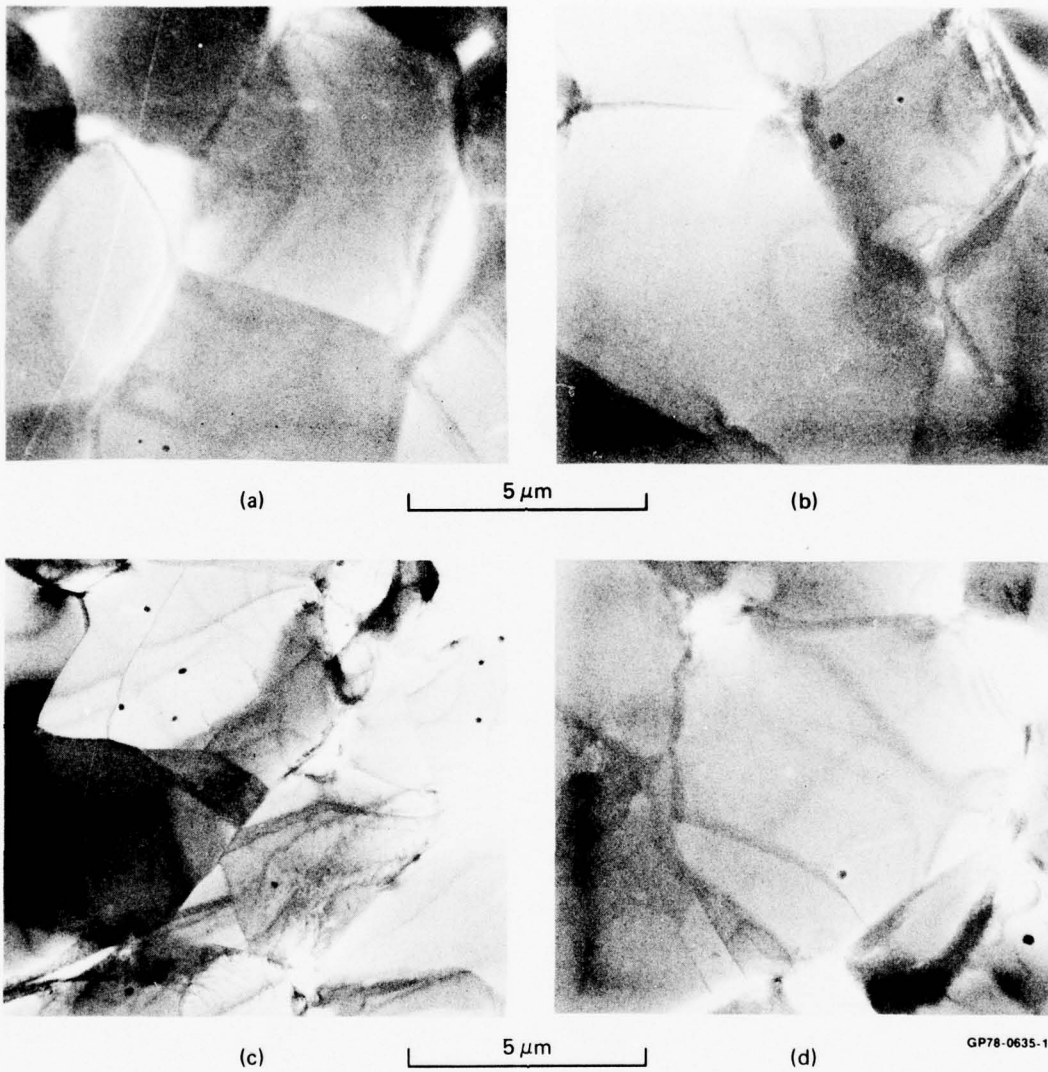
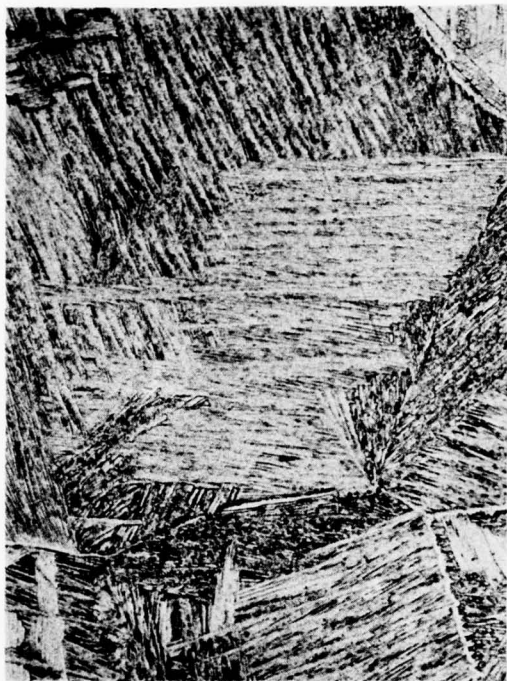


Figure 5. Transmission electron micrographs of alloys processed per schedule A; (a) Ti-6Al-4V reference alloy, (b) Ti-6Al-4V-0.10Er, (c) Ti-6Al-4V-0.05Y, and (d) Ti-6Al-4V-0.038Y₂O₃



(a)

100 μm



(b)



(c)

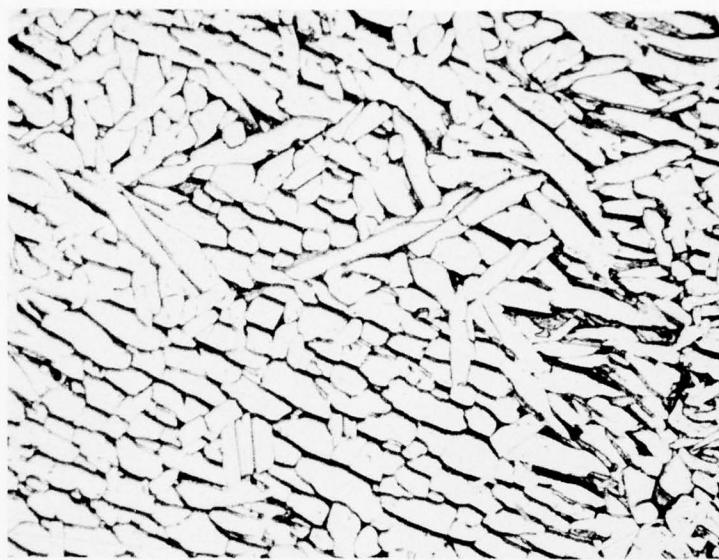
100 μm



(d)

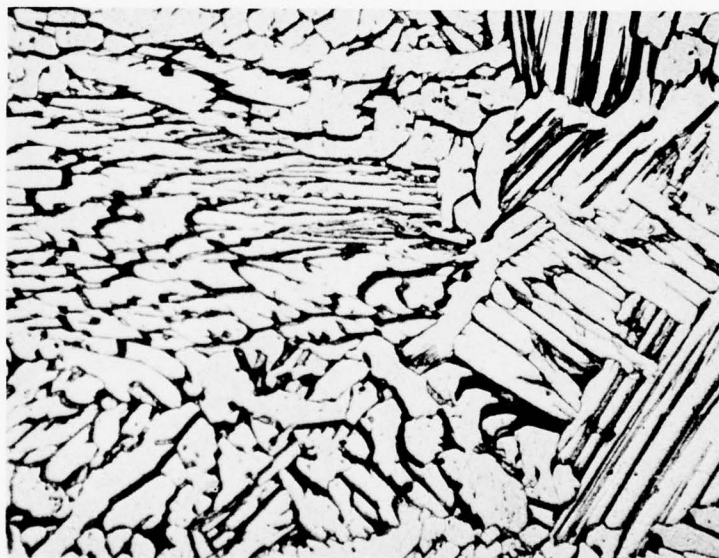
GP78-0635-20

Figure 6. Microstructures of beta-annealed Ti-6Al-4V-RE alloys; (a) Ti-6Al-4V reference alloy, (b) Ti-6Al-4V-0.1Er, (c) Ti-6Al-4V-0.05Y, and (d) Ti-6Al-4V-0.038Y₂O₃



(a)

100 μm



(b)

100 μm

GP78-0635-21

Figure 7. Microstructures of (a) Ti-6Al-4V reference alloy and (b) Ti-6Al-4V-0.02Y alloy processed per schedule B and recrystallization annealed

4. CRYSTALLOGRAPHIC TEXTURE

The crystallographic textures of the hot-rolled, beta-annealed, recrystallization annealed, and solution-treat-and-overaged Ti-6Al-4V-RE alloys were determined by x-ray pole-figure goniometry. The texture development in the alloys was studied by analyzing (0002) and (10 $\bar{1}$ 0) pole figures of the 3.2-mm thick sheets.

The major texture components in the alloys processed per schedule A are near-basal and near-transverse-basal (Figure 8). The deformation texture is unaffected by the rare-earth additions. Beta annealing results in a loss of transverse-basal texture components and the development of a basal texture-component (Figure 9). Annealing in the $\alpha+\beta$ field increases the sharpness of the near-transverse-basal texture components in the Y- and Y₂O₃-containing alloys (Figures 10 and 11).

Alloys rolled per schedule B exhibit stronger basal texture components (Figure 12), and annealing in the $\alpha+\beta$ field sharpens the basal texture (Figure 13).

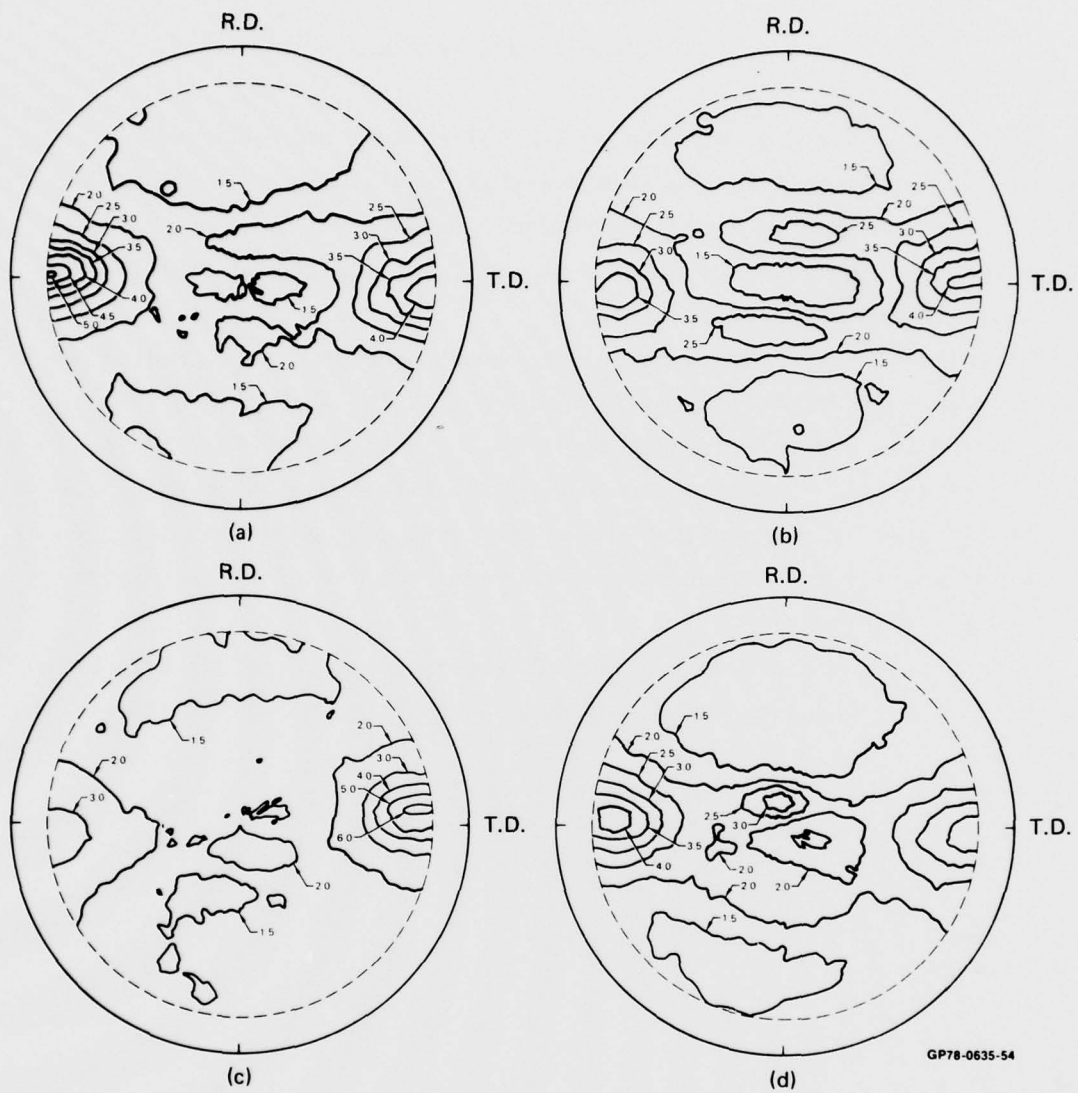
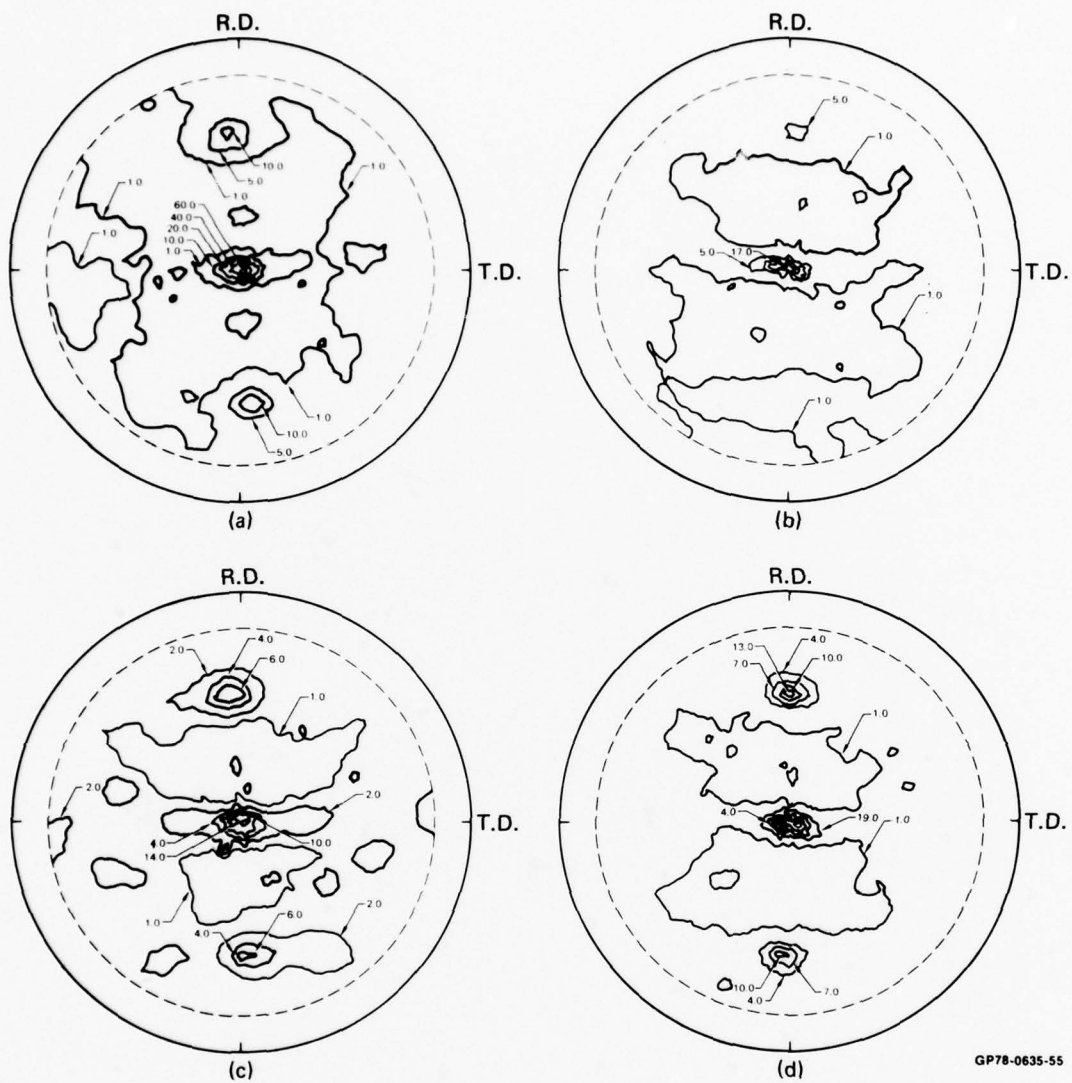
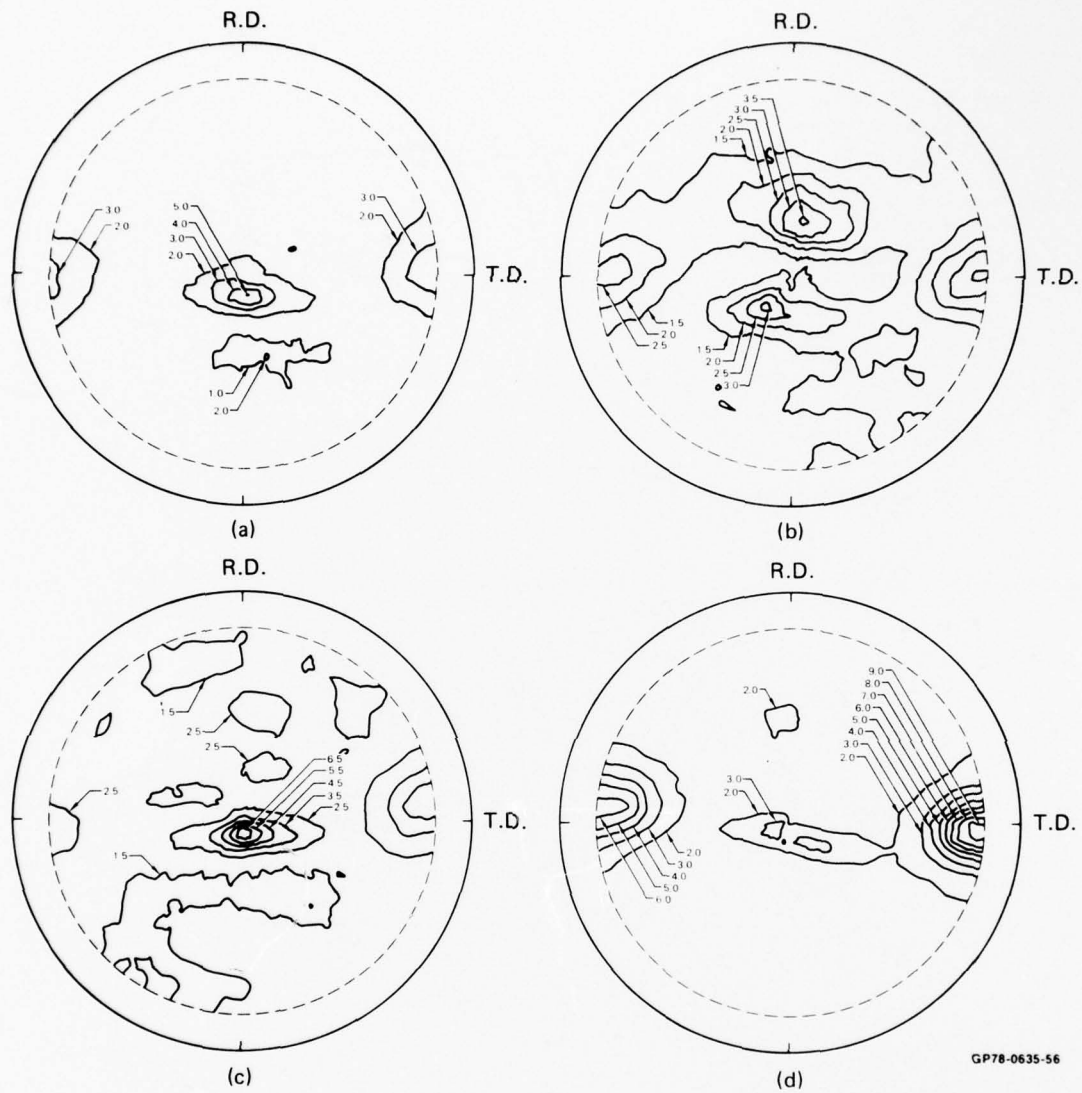


Figure 8. Texture development in alloys processed per schedule A; (a) Ti-6Al-4V reference alloy, (b) Ti-6Al-4V-0.1Er, (c) Ti-6Al-4V-0.05Y, and (d) Ti-6Al-4V-0.038Y₂O₃; (0002) pole figures are shown



GP78-0635-55

Figure 9. Effects of beta annealing on texture of Ti-6Al-4V-RE alloys; (a) Ti-6Al-4V reference alloy, (b) Ti-6Al-4V-0.1Er, (c) Ti-6Al-4V-0.05Y, and (d) Ti-6Al-4V-0.038Y₂O₃; (0002) pole figures are shown



GP78-0635-56

Figure 10. Effect of recrystallization annealing on texture of Ti-6Al-4V-RE alloys; (a) Ti-6Al-4V reference alloy, (b) Ti-6Al-4V-0.1Er, (c) Ti-6Al-4V-0.05Y, and (d) Ti-6Al-4V-0.038Y₂O₃; (0002) pole figures are shown

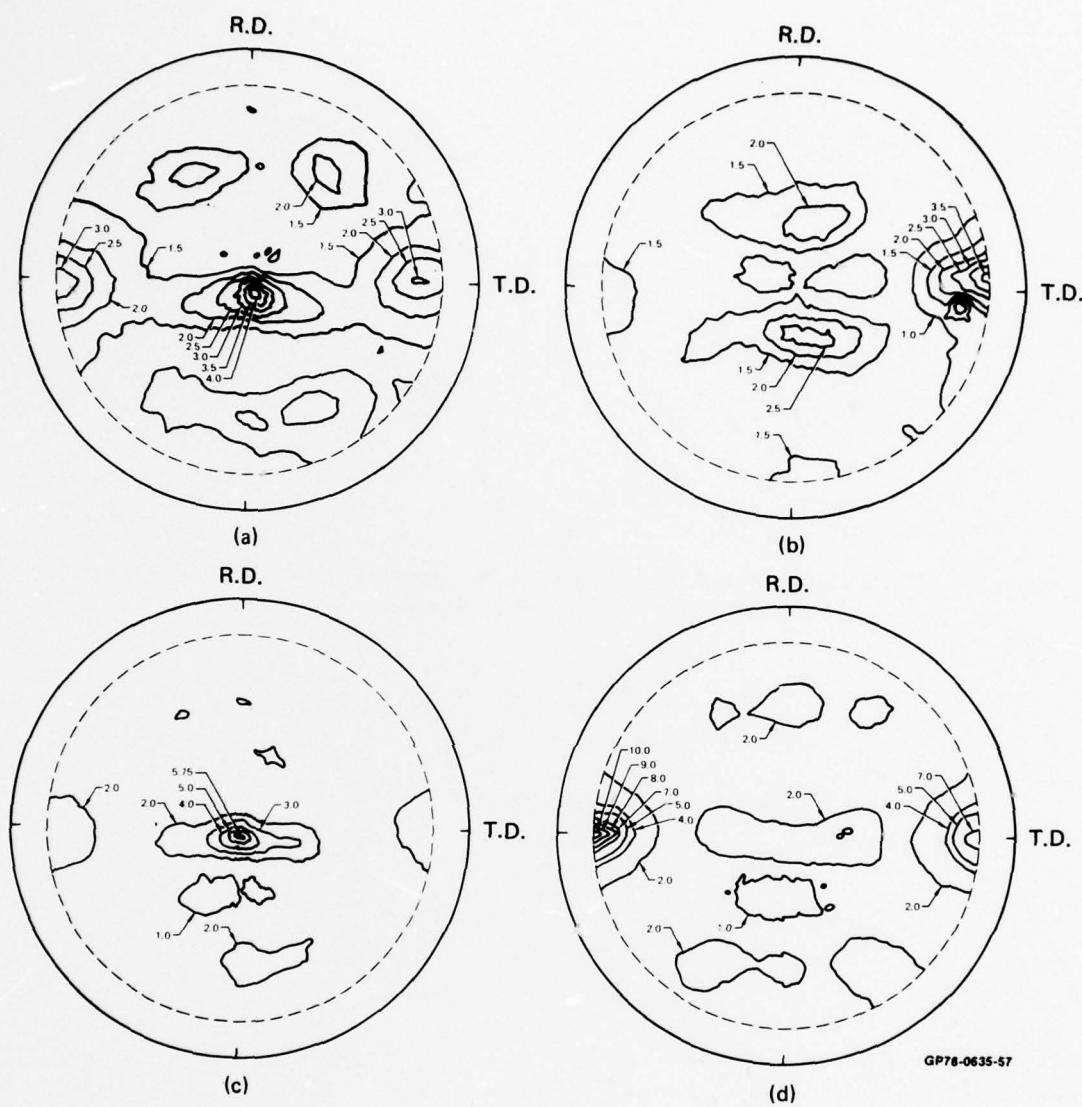


Figure 11. Effect of solution-treatment-and-overaging on texture of Ti-6Al-4V-RE alloys; (a) Ti-6Al-4V reference alloy, (b) Ti-6Al-4V-0.1Er, (c) Ti-6Al-4V-0.05Y, and (d) Ti-6Al-4V-0.038Y₂O₃; (0002) pole figures are shown

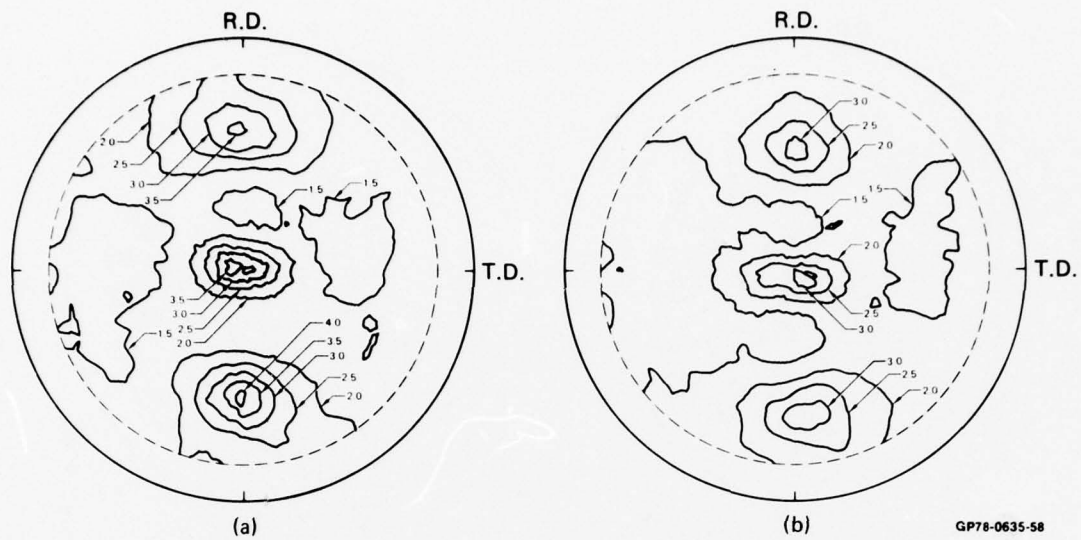


Figure 12. Texture development in alloys processed per schedule B; (a) Ti-6Al-4V-0.05Y and (b) Ti-6Al-4V-0.038Y₂O₃: (10 $\bar{1}$ 0) pole figures are shown

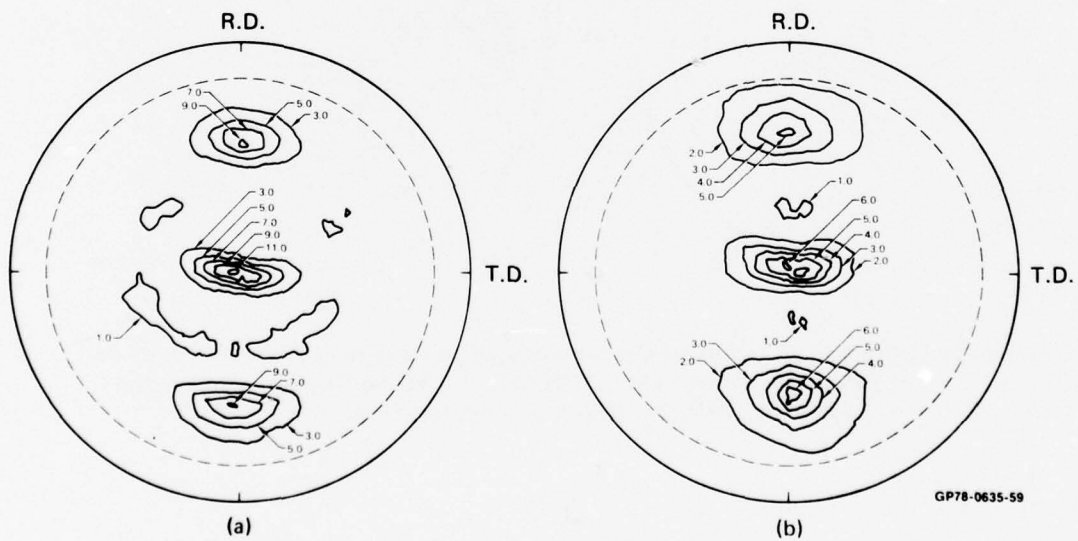


Figure 13. Effect of recrystallization annealing on texture of alloys processed as per schedule B; (a) Ti-6Al-4V-0.05Y and (b) Ti-6Al-4V-0.038Y₂O₃: (10 $\bar{1}$ 0) pole figures are shown

5. ROOM-TEMPERATURE TENSILE PROPERTIES

The room-temperature mechanical properties of the Phase-II Ti-6Al-4V-RE alloys were completely characterized for each of the conventional annealing treatments. Longitudinal and transverse tensile specimen blanks were machined from 13-mm thick plates processed according to the schedules A and B defined in Figure 2, encapsulated in quartz tubes under vacuum, and annealed in accordance with the schedules shown in Table 3. Tensile specimens with 8.0 x 6.0 x 3.1-mm gauge sections were machined from the blanks. The room-temperature tensile-properties data for the Phase-II alloys are shown in Figures 14-23 and listed in Tables A1-A6 of Appendix A.

Although for the Phase-I alloys a slight lowering of yield stress and ultimate tensile stress was observed in rare-earth-containing alloys, the Phase-II alloys showed no significant effect on strength by the Er and Y additions. This absence of an effect on strength may be attributable to smaller than nominal RE concentrations in the Phase-II alloys, but additional chemical analyses must be performed to substantiate such a conclusion. There were slight differences in the tensile properties between the Phase-I and Phase-II alloys, which may be due to small chemistry differences. For example, the Phase-II alloys had less total oxygen and nitrogen (≈ 0.13 wt% O and 0.02 wt% N in Phase-II alloys compared with ≈ 0.16 wt% O and 0.03 wt% N in Phase-I alloys), and the Al:V ratio was slightly lower in the Phase II alloys.

For both the Phase-I and Phase-II alloys, the slight yield-stress differences between the reference alloy and alloys containing 0.10 wt% Er and up to 0.05 wt% Y are not significant.

Phase-I and Phase-II alloys with RE additions had slightly higher ductility than the reference alloy for the β -annealed, solution-treat-and-aged, and solution-treat-and-overaged conditions.

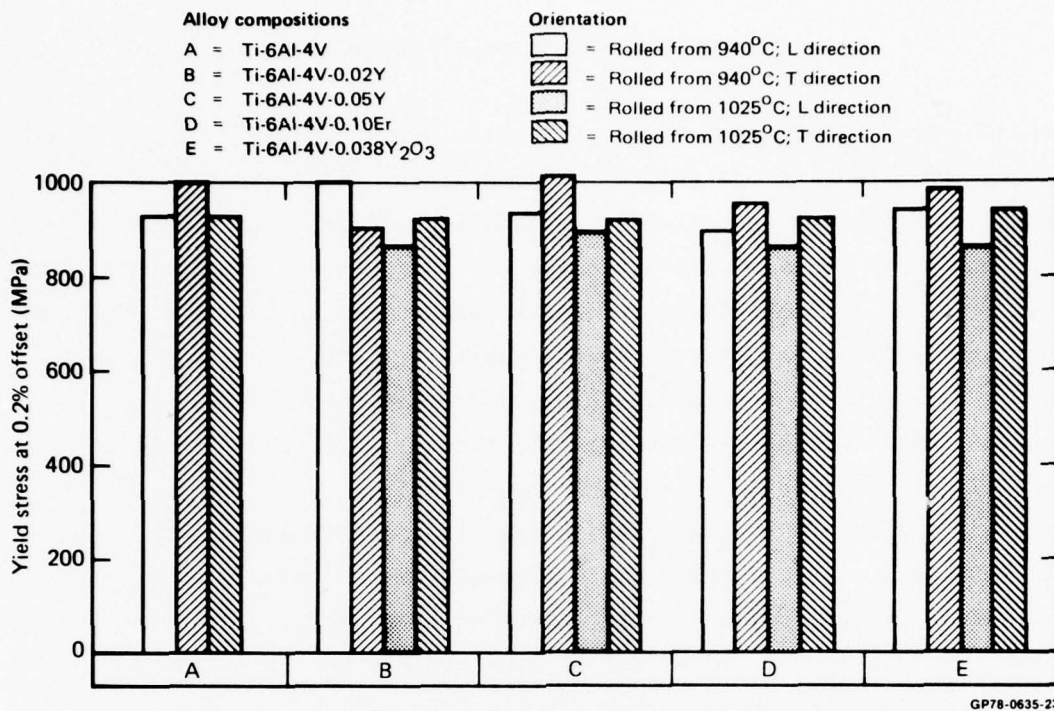


Figure 14. Yield stress of hot-rolled and unannealed Ti-6Al-4V-RE alloys

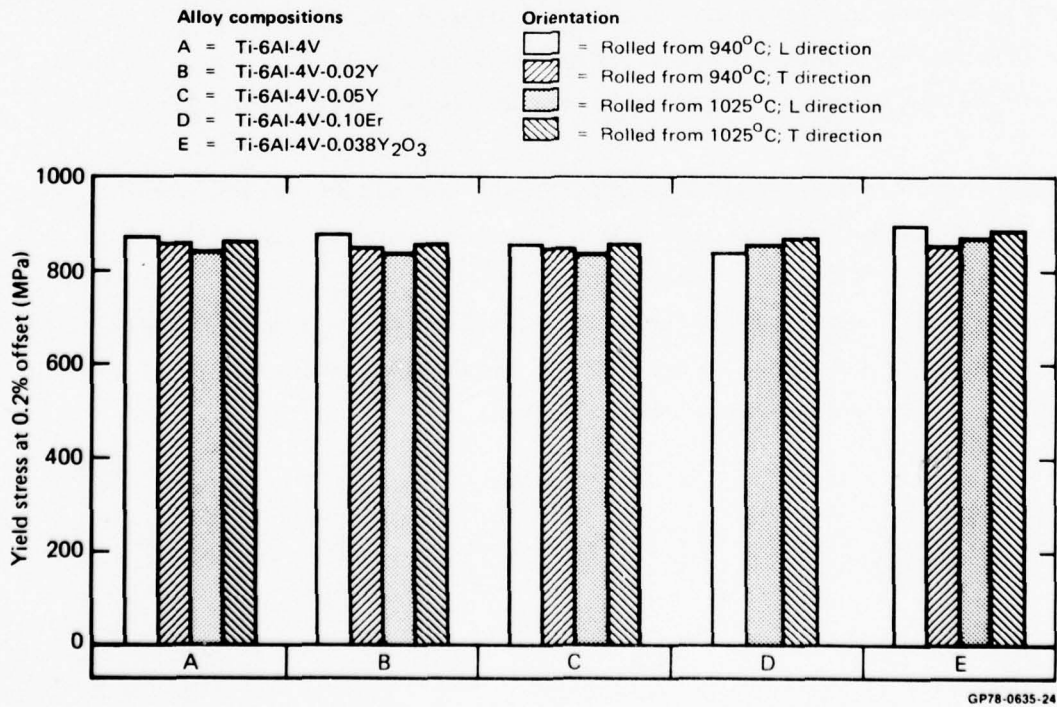


Figure 15. Yield stress of beta-annealed Ti-6Al-4V-RE alloys

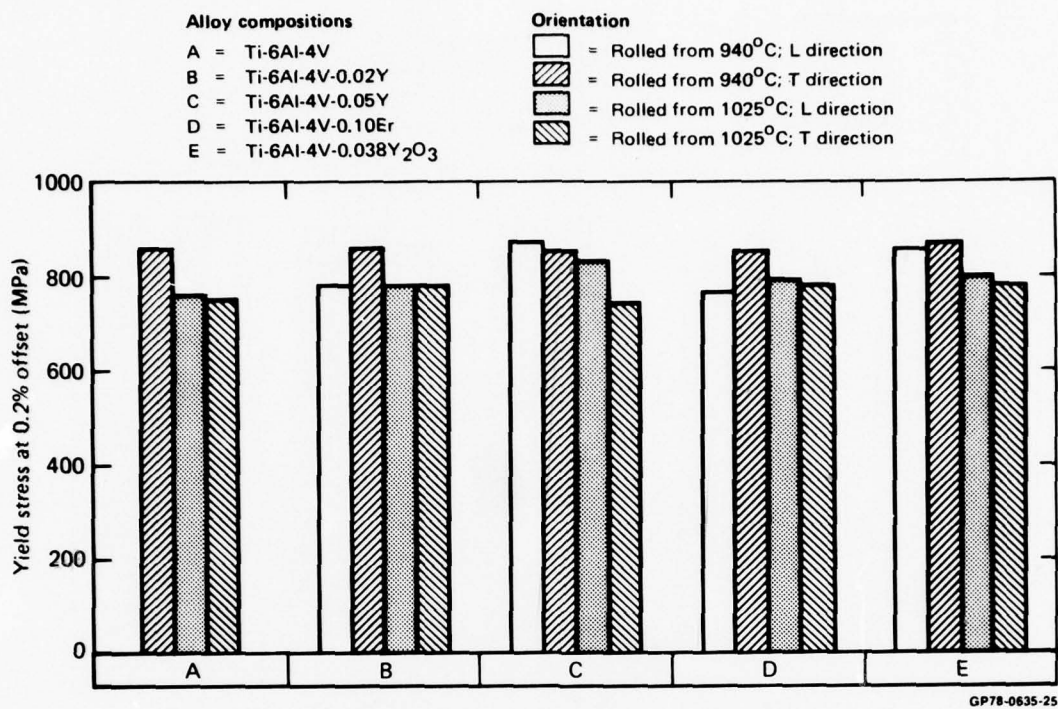


Figure 16. Yield stress of recrystallization annealed Ti-6Al-4V-RE alloys

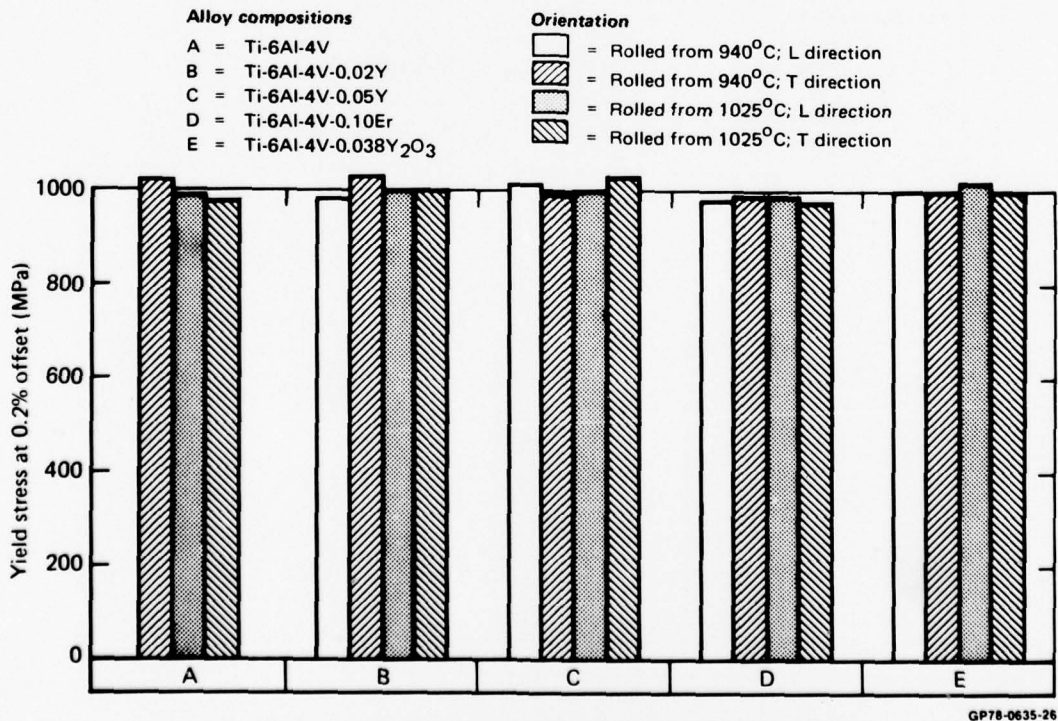


Figure 17. Yield stress of solution-treat-and-overaged Ti-6Al-4V-RE alloys

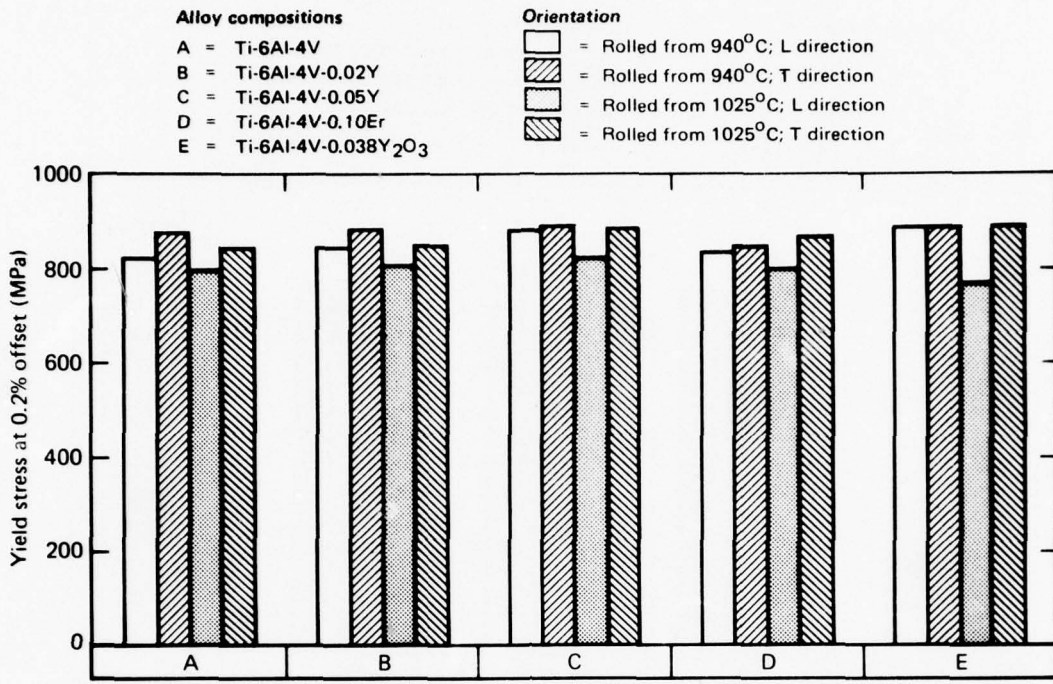


Figure 18. Yield stress of α - β annealed and aged Ti-6Al-4V-RE alloys

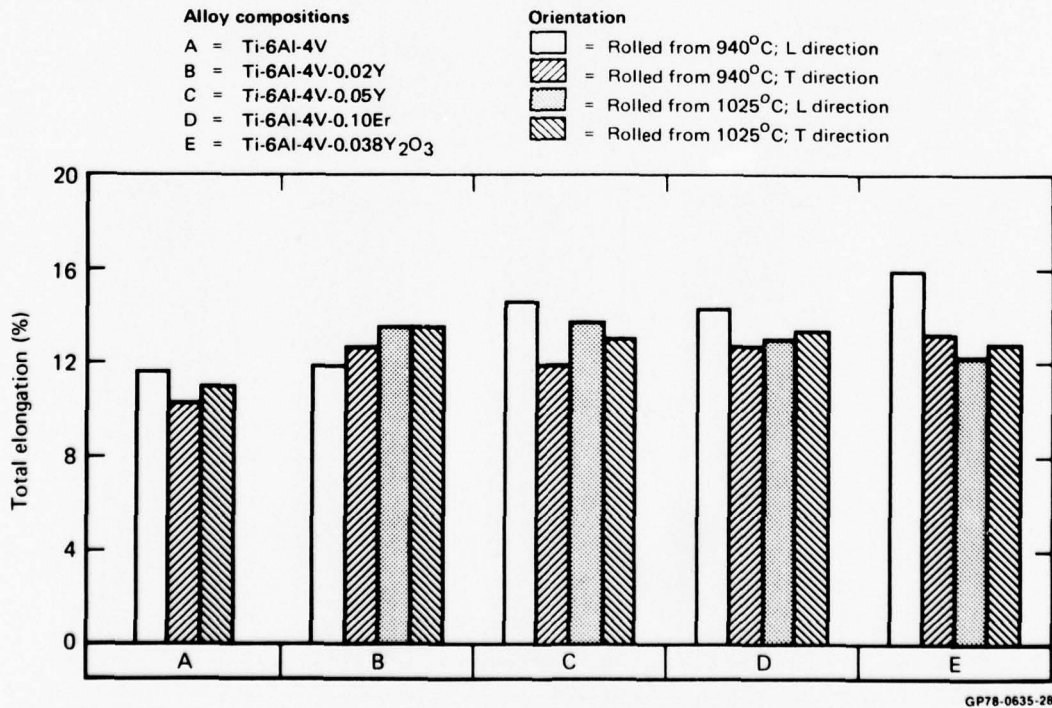


Figure 19. Total elongation of hot-rolled and unannealed Ti-6Al-4V-RE alloys

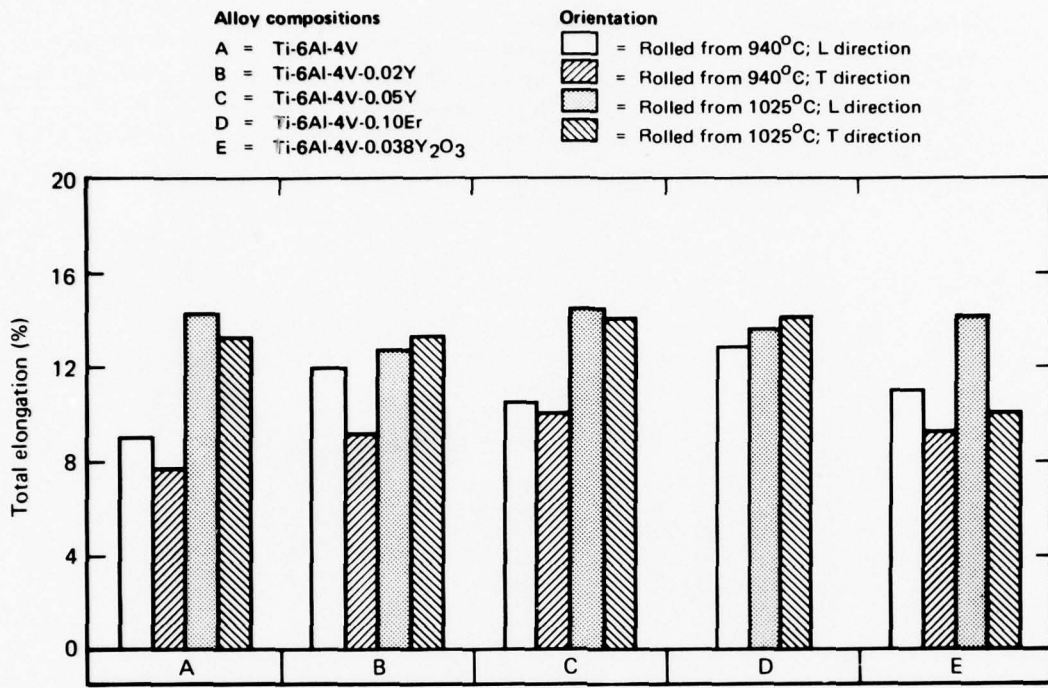


Figure 20. Total elongation of beta-annealed Ti-6Al-4V-RE alloys

GP78-0635-29

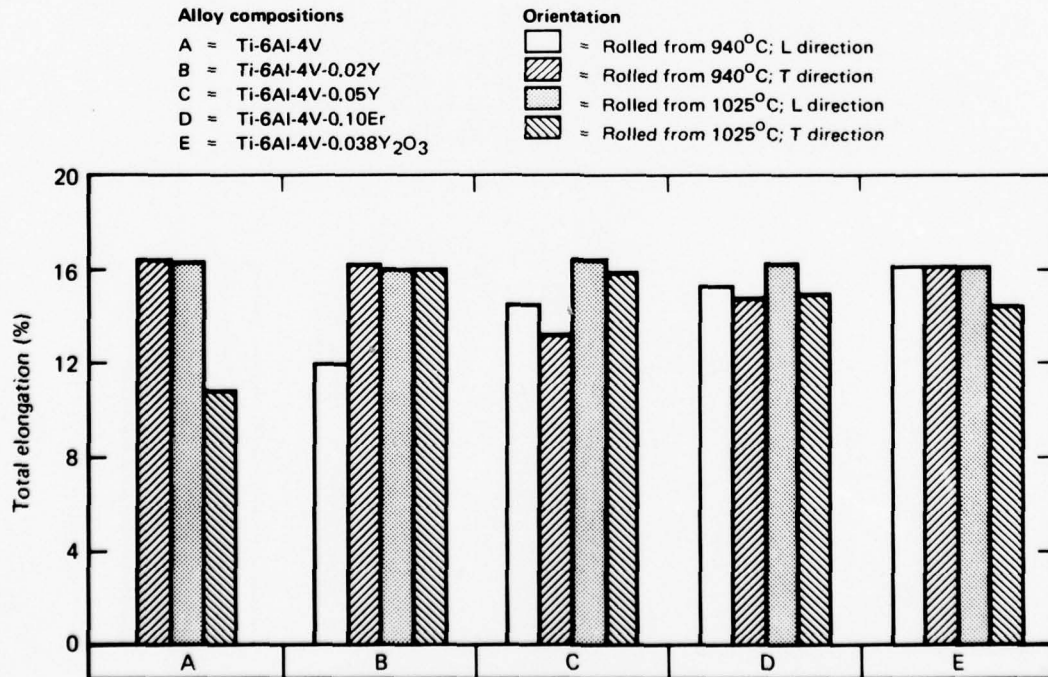


Figure 21. Total elongation of recrystallization annealed Ti-6Al-4V-RE alloys

GP78-0635-30

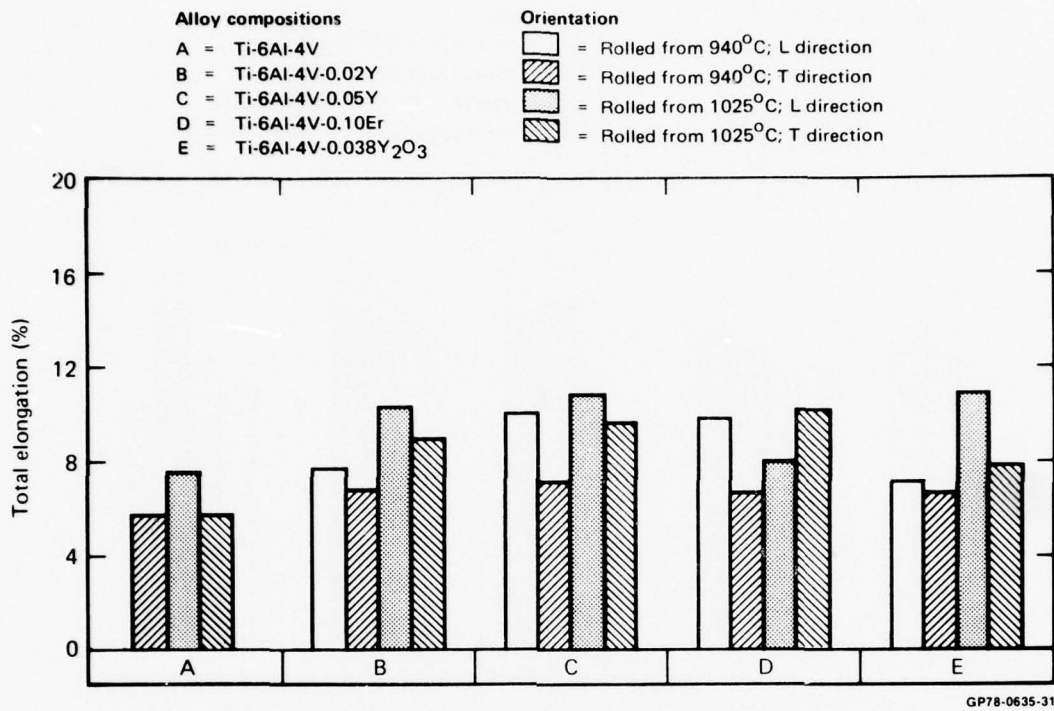


Figure 22. Total elongation of solution-treat-and-overaged Ti-6Al-4V-RE alloys

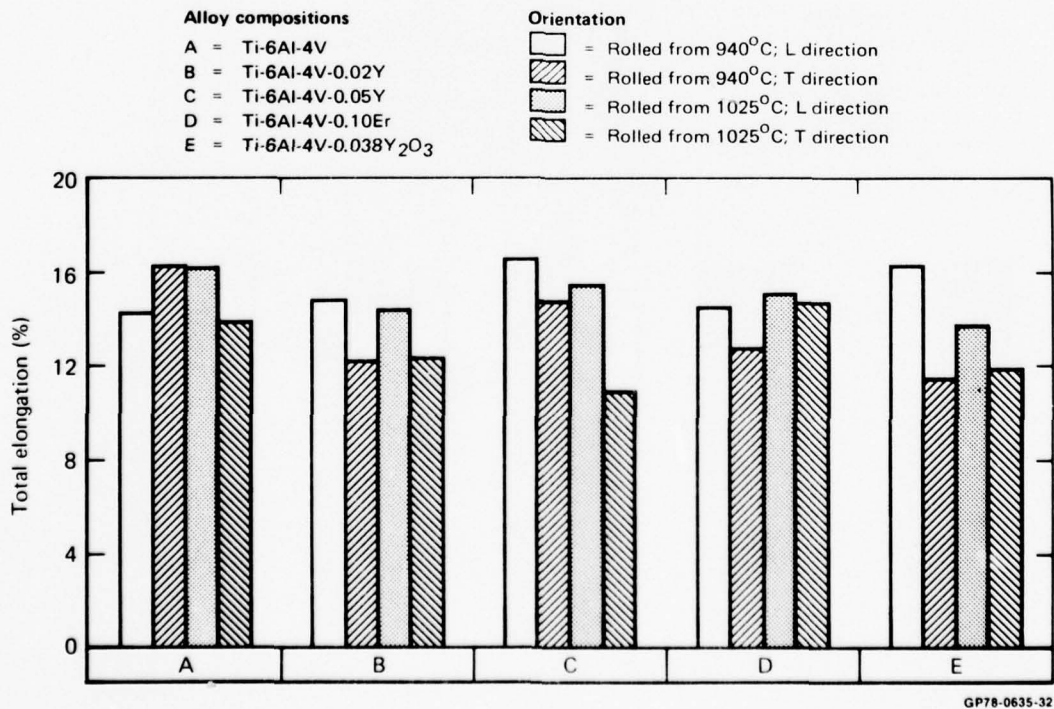


Figure 23. Total elongation of α-β annealed and aged Ti-6Al-4V-RE alloys

6. FRACTURE TOUGHNESS

The fracture toughness (K_Q) values of the alloys were determined from three-point-loaded slow-bend tests of Charpy V-notched and fatigue-precracked specimens. The specimens were tested after the following heat treatments: (1) beta anneal at 1040°C for 0.5 h, air cool to room temperature, stabilization anneal at 700°C for 2 h, and air cool to room temperature; (2) recrystallization anneal at 930°C for 4 h, cool at 55°C/h to 700°C, and air cool to room temperature; and (3) solution-anneal at 955°C for 2 h, water quench, age at 710°C for 4 h, and air cool to room temperature. The room-temperature K_Q values of the Phase-II alloys are shown in Figures 24-29 and listed in Tables A7-A9 of Appendix A.

The solution-treat-and-aged alloys have lower K_Q values than the beta-annealed and recrystallization-annealed alloys. There are no significant differences between the K_Q values of the reference alloy and the rare-earth-containing alloys in the recrystallization-annealed and solution-treat-and-aged conditions; the differences are within the experimental scatter-band characteristic of the test technique. In the beta-annealed condition, the Er- and Y-containing alloys have slightly lower fracture toughness than the reference alloy. The reduced fracture toughness is a consequence of smaller prior-beta-grain size rather than the presence of the rare-earth dispersoids.

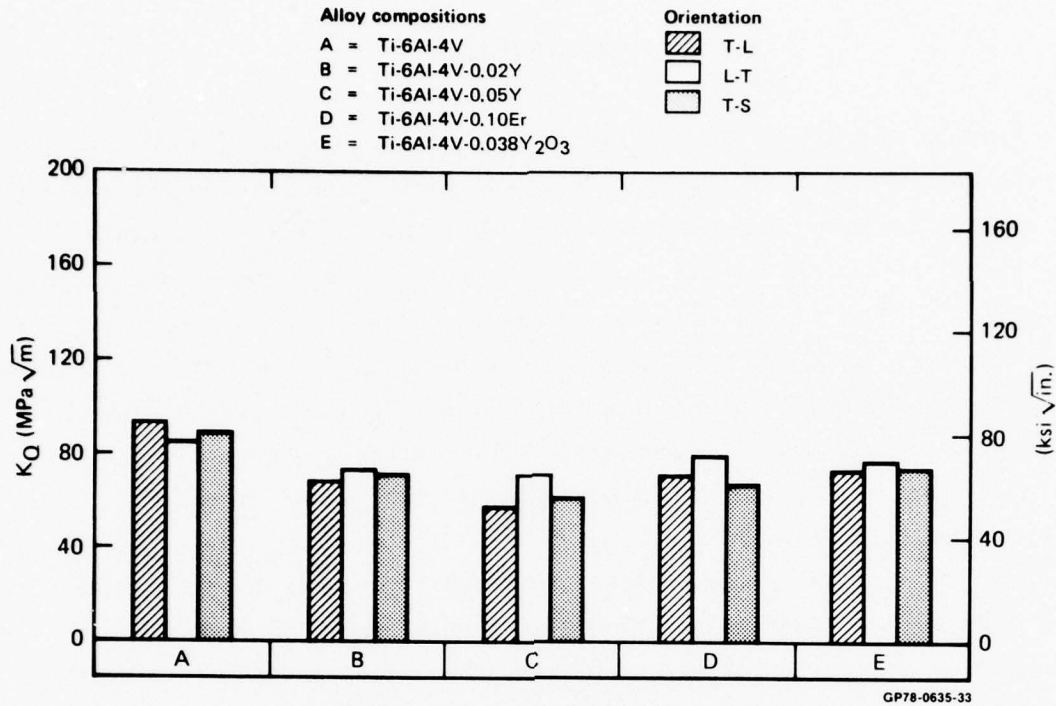


Figure 24. Fracture toughness (K_Q) of beta-annealed Ti-6Al-4V-RE alloys processed according to schedule B

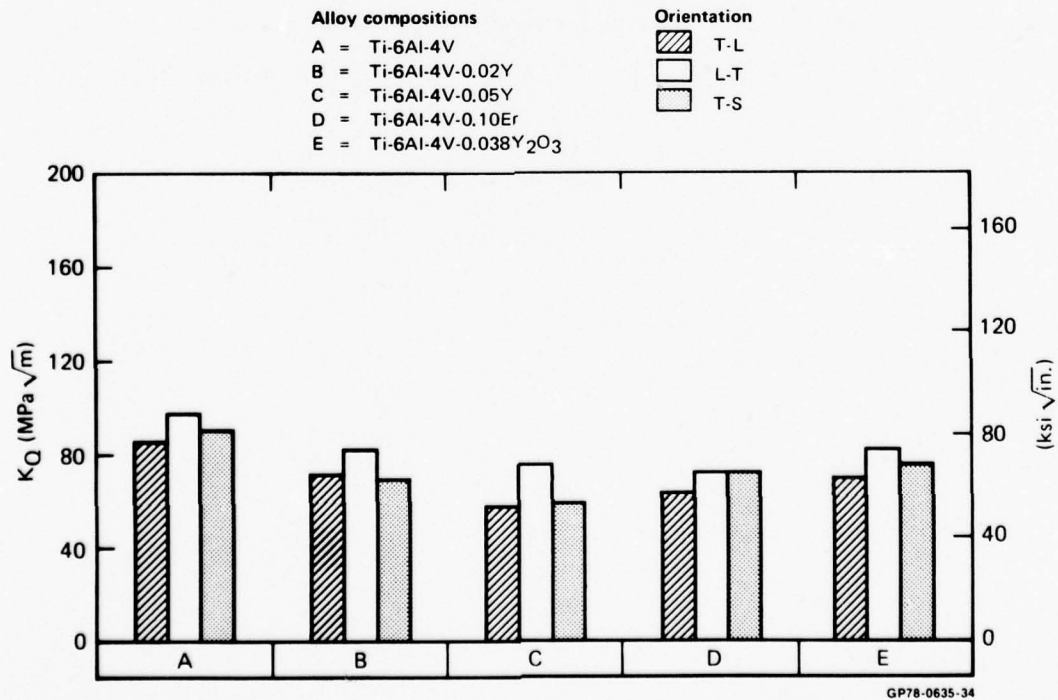


Figure 25. Fracture toughness (K_Q) of beta-annealed Ti-6Al-4V-RE alloys processed according to schedule A

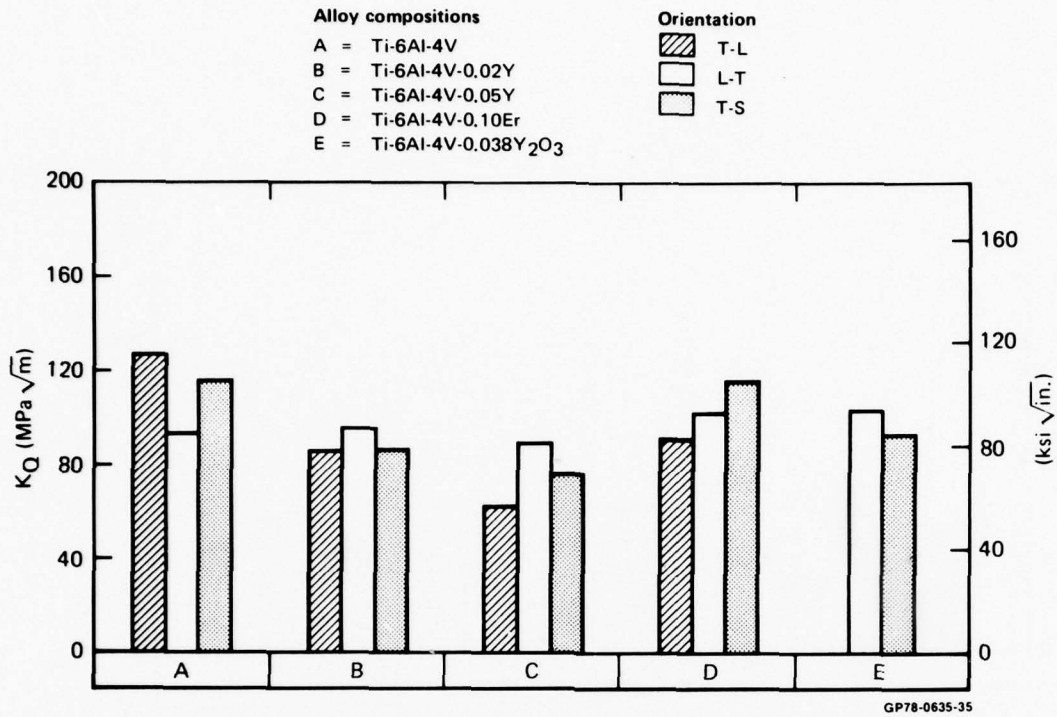


Figure 26. Fracture toughness (K_Q) of recrystallization-annealed Ti-6Al-4V-RE alloys processed according to schedule B

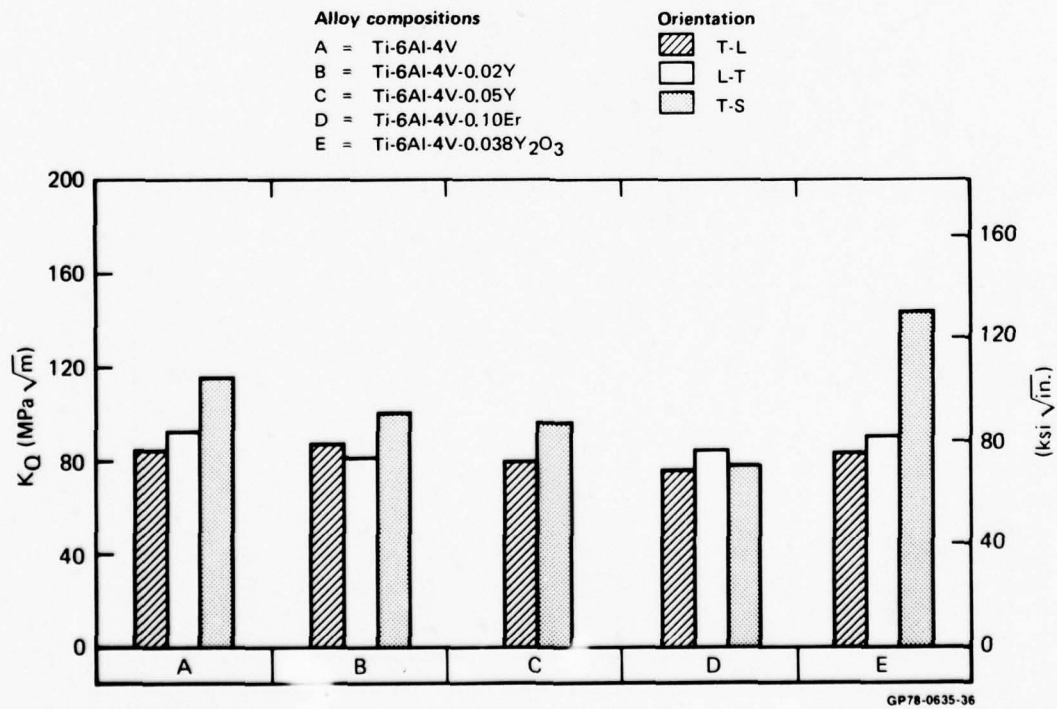


Figure 27. Fracture toughness (K_Q) of recrystallization-annealed Ti-6Al-4V-RE alloys processed according to schedule A

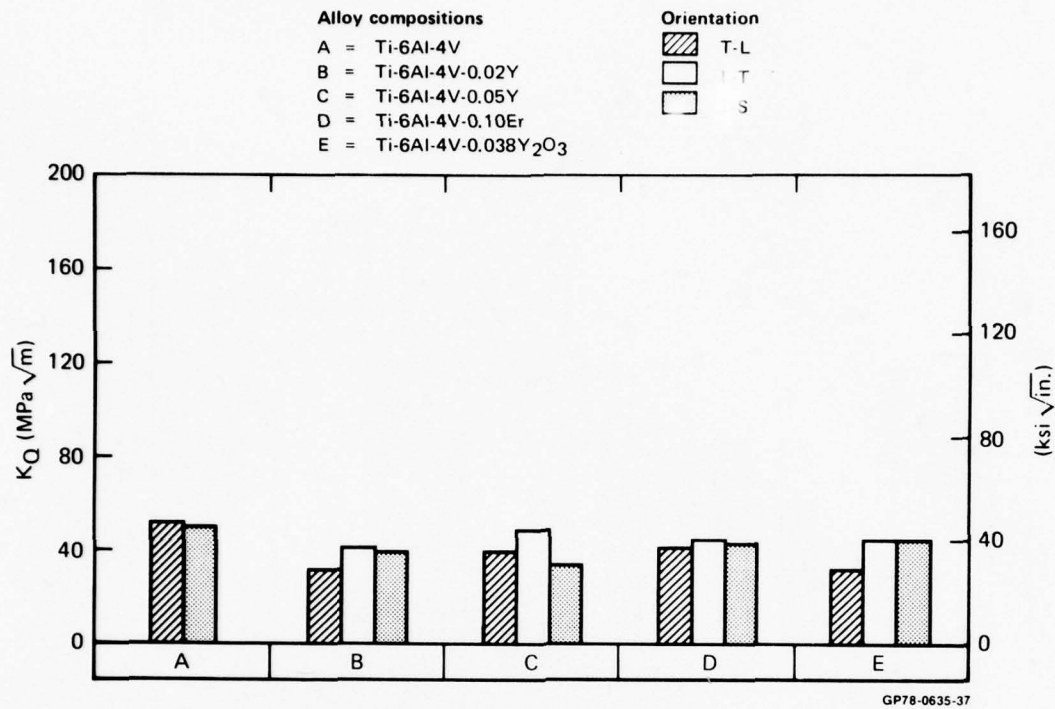


Figure 28. Fracture toughness (K_Q) of solution-treat-and-overaged Ti-6Al-4V-RE alloys processed according to schedule B

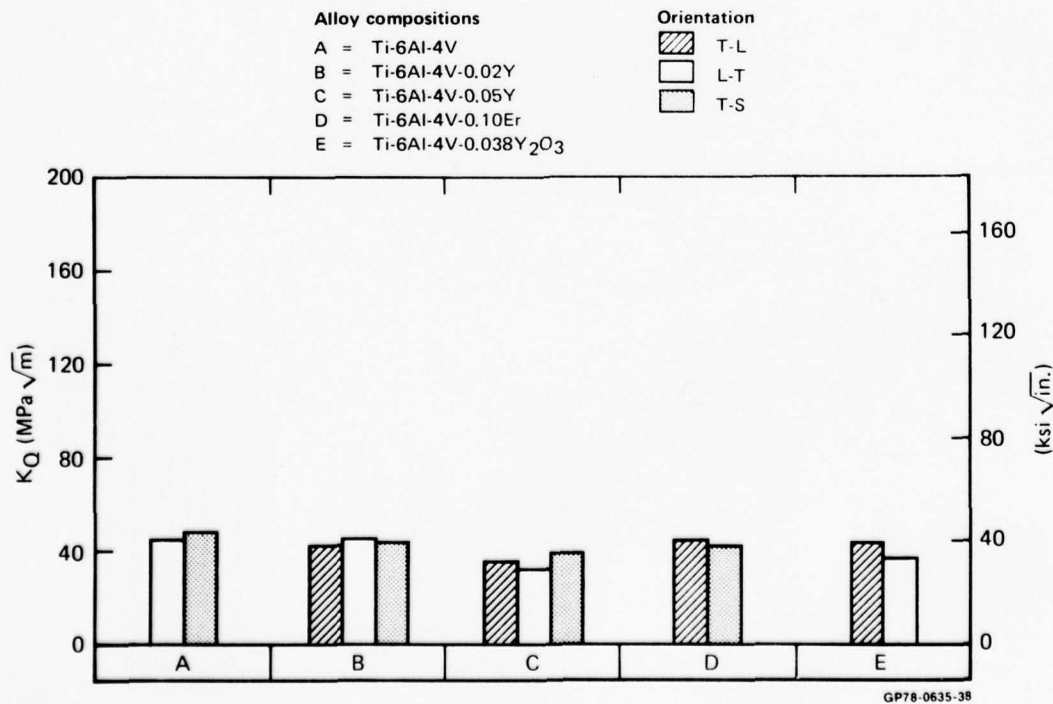


Figure 29. Fracture toughness (K_Q) of solution-treat-and-overaged Ti-6Al-4V-RE alloy processed according to schedule A

7. PLANE-STRESS FRACTURE TOUGHNESS

The fracture toughness, K_Q , under plane-stress conditions was measured on center-cracked tension specimens of the Phase-II Ti-6Al-4V-RE alloys subjected to various heat treatments. The 3.1 x 76 x 203 mm sheet specimens were tested for susceptibility to crack growth in the transverse direction under loading in the longitudinal, or rolling direction.

At present there is no standard method for plane-stress fracture-toughness testing. For the test method chosen for the present investigation, cracks are initiated by fatigue on both sides of a notched hole in the center of the specimen, the specimen is then pulled in tension and the half-crack length is recorded as a function of applied tensile load. Figure 30 shows the specimen geometry and test set-up. The stress intensity, full-section stress, and half-crack length for the given sample geometry are related in accordance with the expression

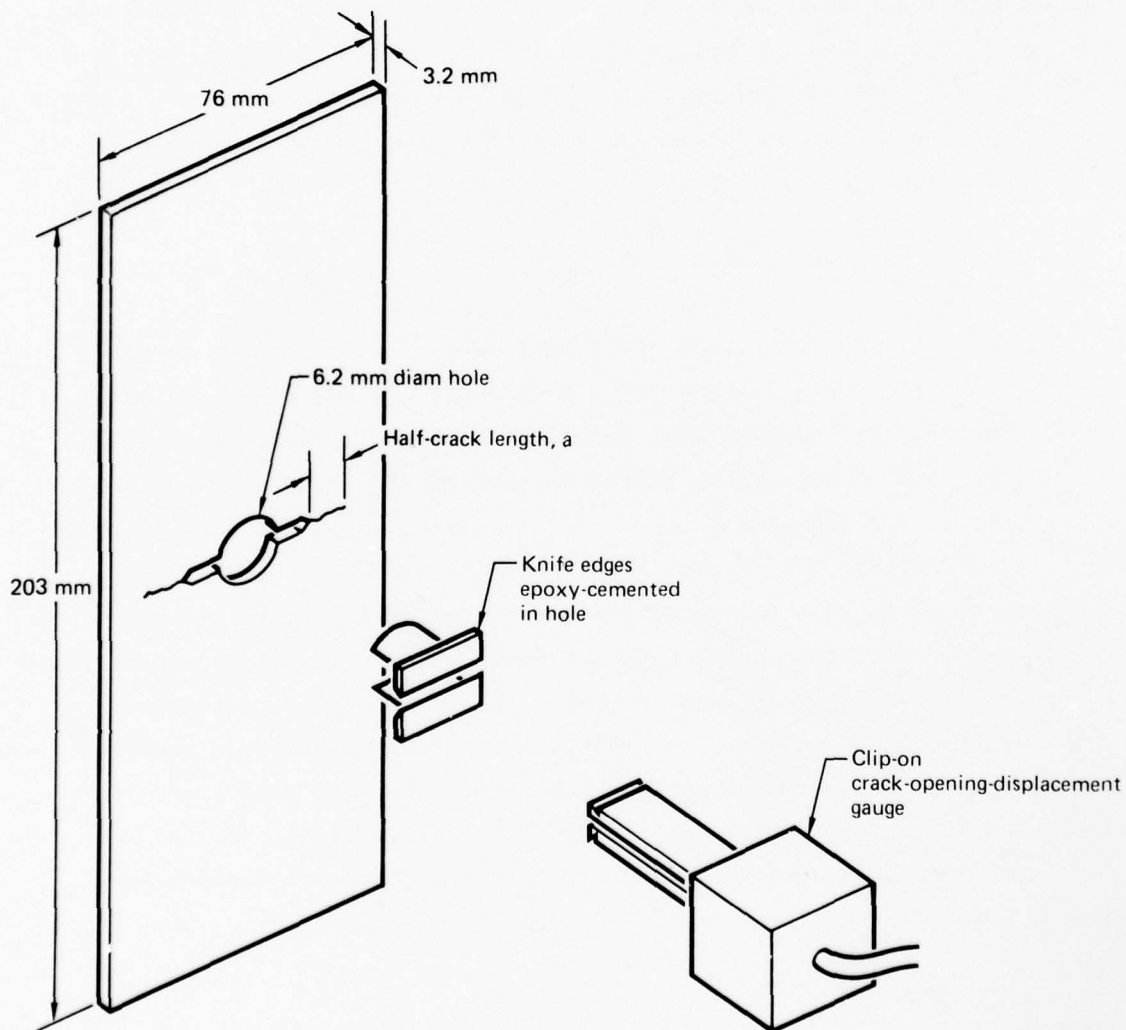
$$K = \sigma \sqrt{\pi a Z} , \quad (1)$$

where σ is the full-section stress (load divided by total cross-sectional area), a is the half-crack length, and $Z = \sec(\pi a/w)$ is the finite-width correction factor. The plane-stress fracture-toughness is defined as that value of K for which crack growth becomes unstable. Because under plane-stress, significant crack growth occurs before instability, the instantaneous, rather than the initial, half-crack length must be used. For each alloy heat treatment, there is a unique relationship, called the crack-growth-resistance curve, between crack length and the applied stress-intensity factor. Instability arises when the stress intensity at the crack tip, defined by Equation (1), increases more rapidly than the material response as given by the crack-growth-resistance curve. The following equation, developed by Forman⁶ and modified to account for the finite specimen width, relates the instantaneous half-crack length to the applied load and crack opening as measured by a vertical-displacement gauge:

$$aZ = \frac{C\pi E}{2 \sigma_{y.s.} \ln \left(\frac{\sin\beta + 1}{\sin\beta - 1} \right)^2} , \quad (2)$$

where C is the vertical displacement as measured by a crack-opening-displace-

ment gauge, E is the elastic modulus of the material, $\sigma_{y.s.}$ is the yield strength of the material, and $\beta = (\pi/2)(\sigma/\sigma_{y.s.})$. The crack-growth-resistance curve is obtained by using Equation (2) to calculate a half-crack length for a given load and crack-opening, and then employing Equation (1) to calculate the stress intensity associated with this half-crack length and applied load. The fracture toughness value is obtained by locating the point of tangency between the crack-growth-resistance curve and an applied-stress-intensity curve of the appropriate value of applied load, as shown schematically in Figure 31.



GP78-0635 60

Figure 30. Specimen geometry and mounting of crack-opening-displacement gauge for measurement of plane-stress fracture-toughness

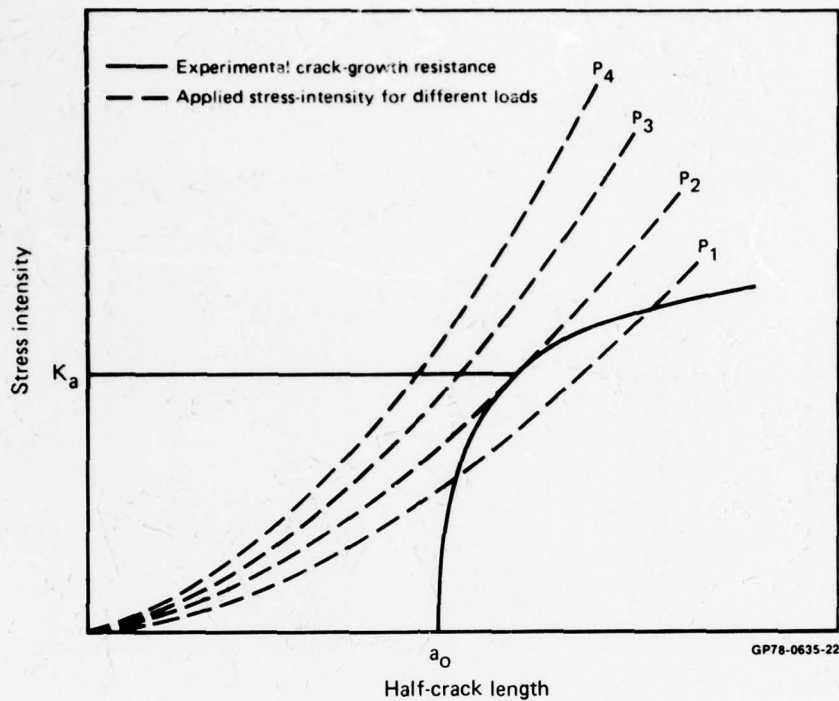


Figure 31. Schematic representation of plane-stress fracture-toughness determination

The fracture toughness values determined by this method for the alloys, rolling schedules, and heat treatments of this study are shown in Figures 32-34 and listed in Table A10 of Appendix A. The beta-annealed alloys generally have the highest fracture toughness. There are no significant differences between the K_Q values of the reference alloy and the rare-earth containing alloys in the recrystallization-annealed and solution-treat-and-aged condition. However, in the beta-annealed condition, rare-earth-containing alloys have a slightly higher fracture toughness than the reference alloy in contrast with the result of slow-bend, plane-strain tests on the same alloys described in Section 6.

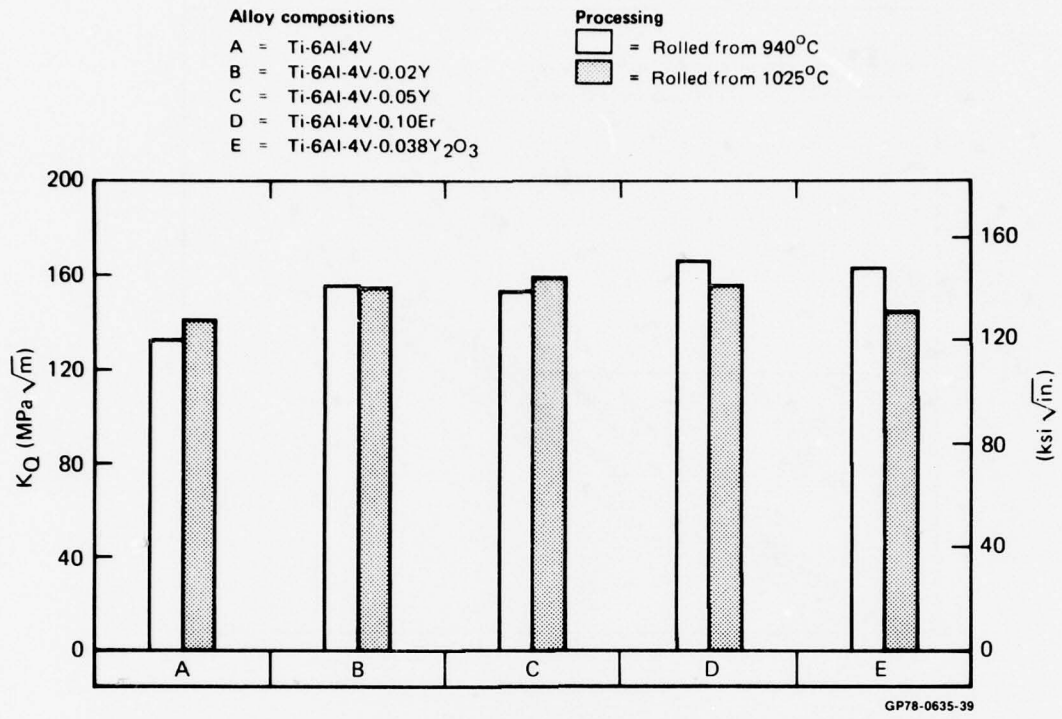


Figure 32. Plane-stress fracture toughness of beta-annealed Ti-6Al-4V-RE alloys

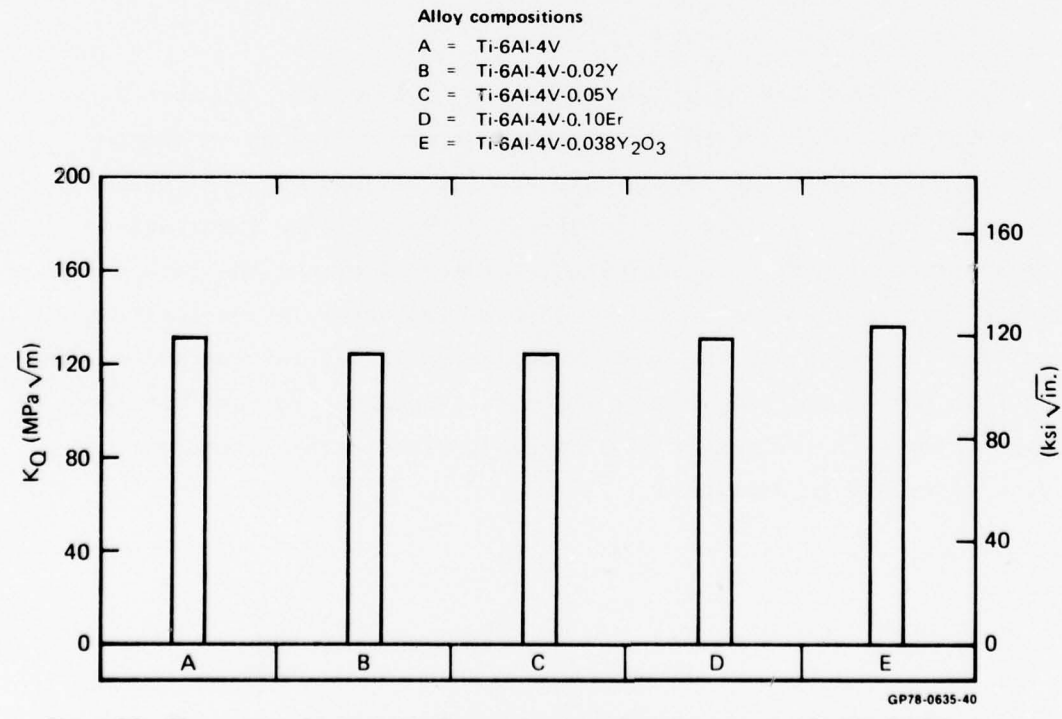


Figure 33. Plane-stress fracture toughness of recrystallization-annealed Ti-6Al-4V-RE alloys processed according to schedule A

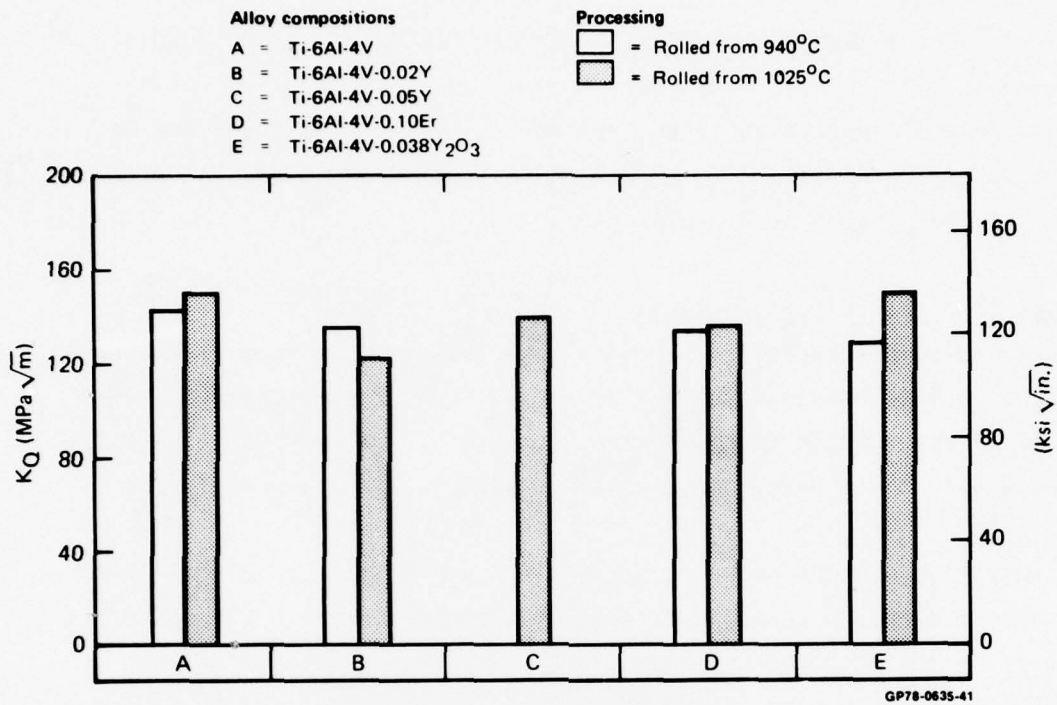


Figure 34. Plane-stress fracture toughness of solution-treat-and-overaged Ti-6Al-4V-RE alloys

8. HIGH-TEMPERATURE DEFORMATION OF PHASE-II Ti-6Al-4V-RE ALLOYS

Tensile and compression tests from 700° to 950°C were performed on Phase-II Ti-6Al-4V-RE alloys to determine temperatures and strain rates to be used for the next phase of this study.

8.1 High-Temperature Tensile Tests

The high-temperature tensile tests were performed on samples heated in air to the desired temperature in a three-zone quartz-lamp furnace. The test samples were heated to the desired temperature at the rate of 100°C/s, and the tensile tests were conducted at initial strain rates of 0.01 s⁻¹ and 0.1 s⁻¹.

Figures 35a and 35b show the photographs of two sets of Ti-6Al-4V-RE alloys deformed 40% in tension at 870°C at an initial strain rate of 0.1 s⁻¹. The set of Y- and Er-containing alloys shown in Figure 35a had uniform elongation without necking, whereas the Ti-6Al-4V reference alloy exhibited significant necking. When the tests were repeated on the set of Ti-6Al-4V-RE alloys shown in Figure 35b, the Er-containing alloy also exhibited necking, possibly because the sample contained little Er as a result of a non-uniform Er-distribution in the rolled plate. However, minute inhomogeneities on specimen surfaces can cause premature necking in the high-temperature tensile tests, and although the results of the above tests are indicative, they are not conclusive.

The details of the $\alpha+\beta$ microstructure of the Ti-6Al-4V specimen deformed at 800°C at a strain rate of 0.1 s⁻¹ are shown in Figure 36. The deformation structure consists of Widmanstätten $\alpha-\beta$ plates with high aspect-ratios. An important feature of the deformed structures is the presence of the "interface phase", shown in the dark-field micrograph in Figure 36d. Extensive dislocation activity can be seen in the alpha phase.

The effects of temperature and strain rate on the substructure are shown in Figures 37a-37d. The undeformed specimens consist of fine, equiaxed, primary alpha and grain-boundary beta. The specimens deformed at 800°C and 850°C and subsequently cooled at a fast rate consist of primary alpha and Widmanstätten $\alpha-\beta$ plates. The morphology of the $\alpha-\beta$ plates reflects the deformation history of the β phase at the test temperature. Whereas there is only one dominant orientation of β plates in the specimens at 800°C, the

specimens deformed at 850°C consist of β plates of at least two different orientations. The interface phase in specimens deformed at 800°C is wider for the slow strain rate of 0.01 s^{-1} than for 0.1 s^{-1} . The α - β morphology is a consequence of both thermal history and deformation history of the specimens.

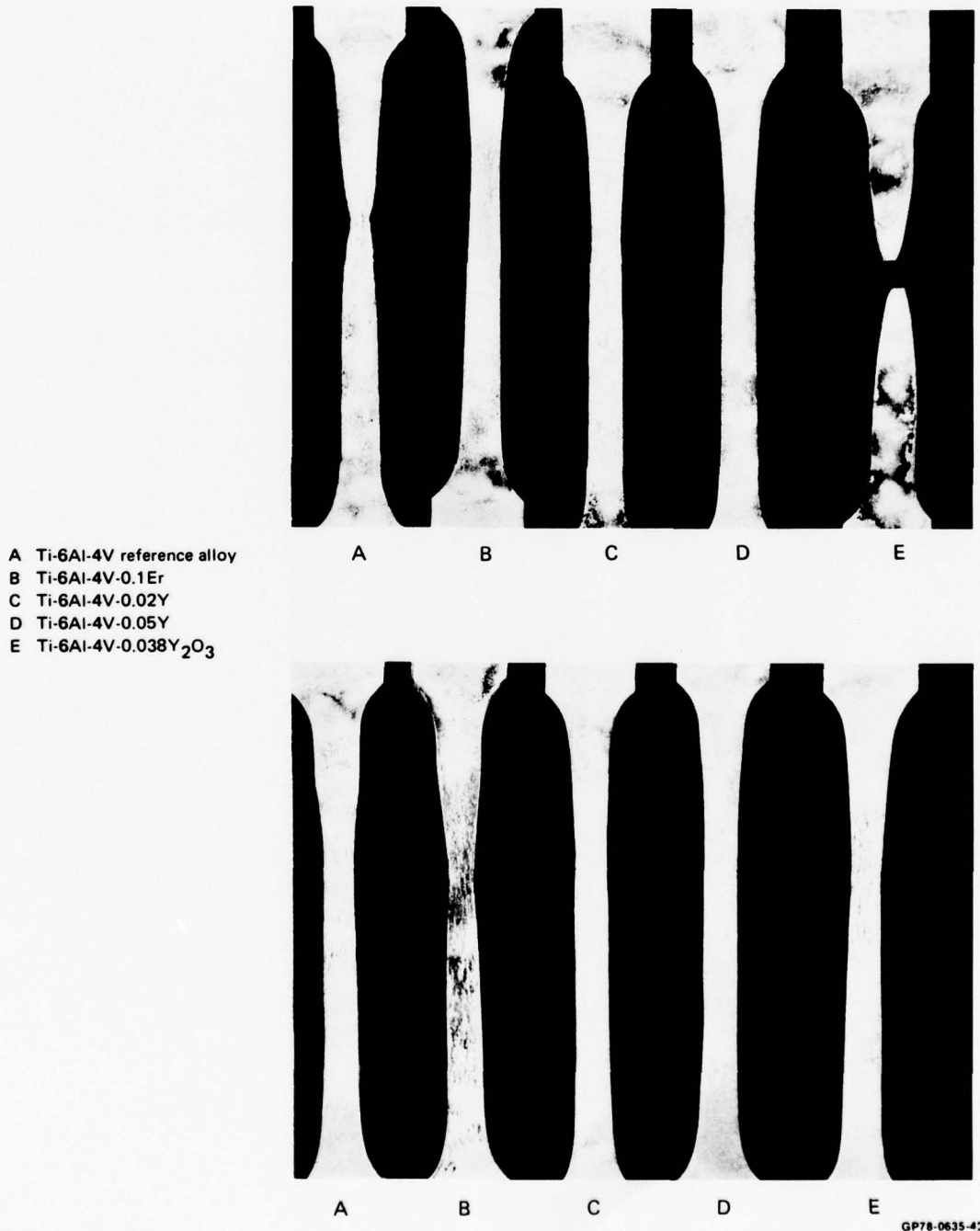
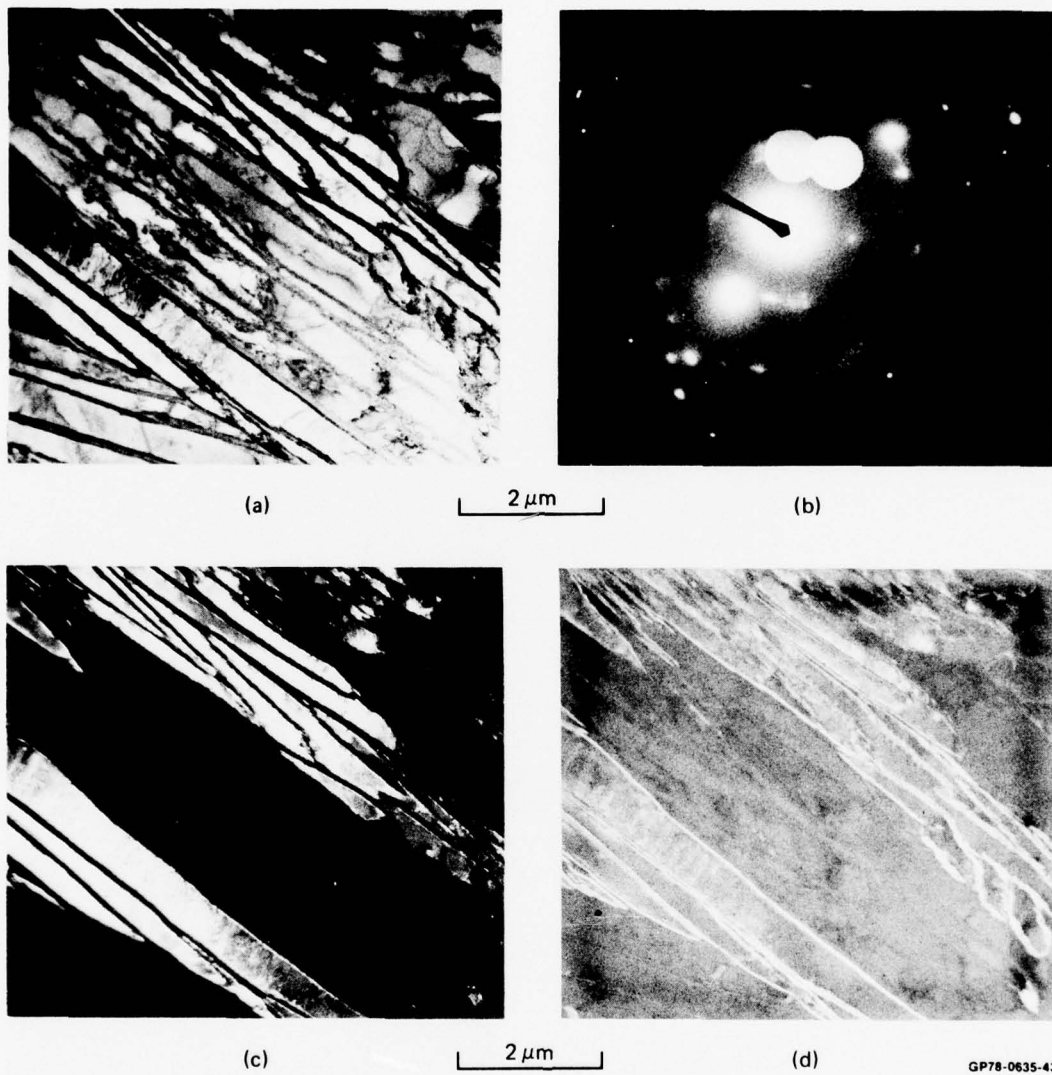


Figure 35. Photographs of two sets of Ti-6Al-4V-RE alloys processed per schedule B and deformed 40% in tension at 870°C at a strain rate of 0.1 s^{-1}



GP78-0635-43

Figure 36. Details of α - β microstructure observed in Ti-6Al-4V specimens deformed at 800°C at a strain rate of 0.1 s⁻¹; (a) bright-field electron micrograph, (b) selected-area diffraction pattern, (c) dark-field electron micrograph with α reflection, and (d) dark-field electron micrograph of the interface phase

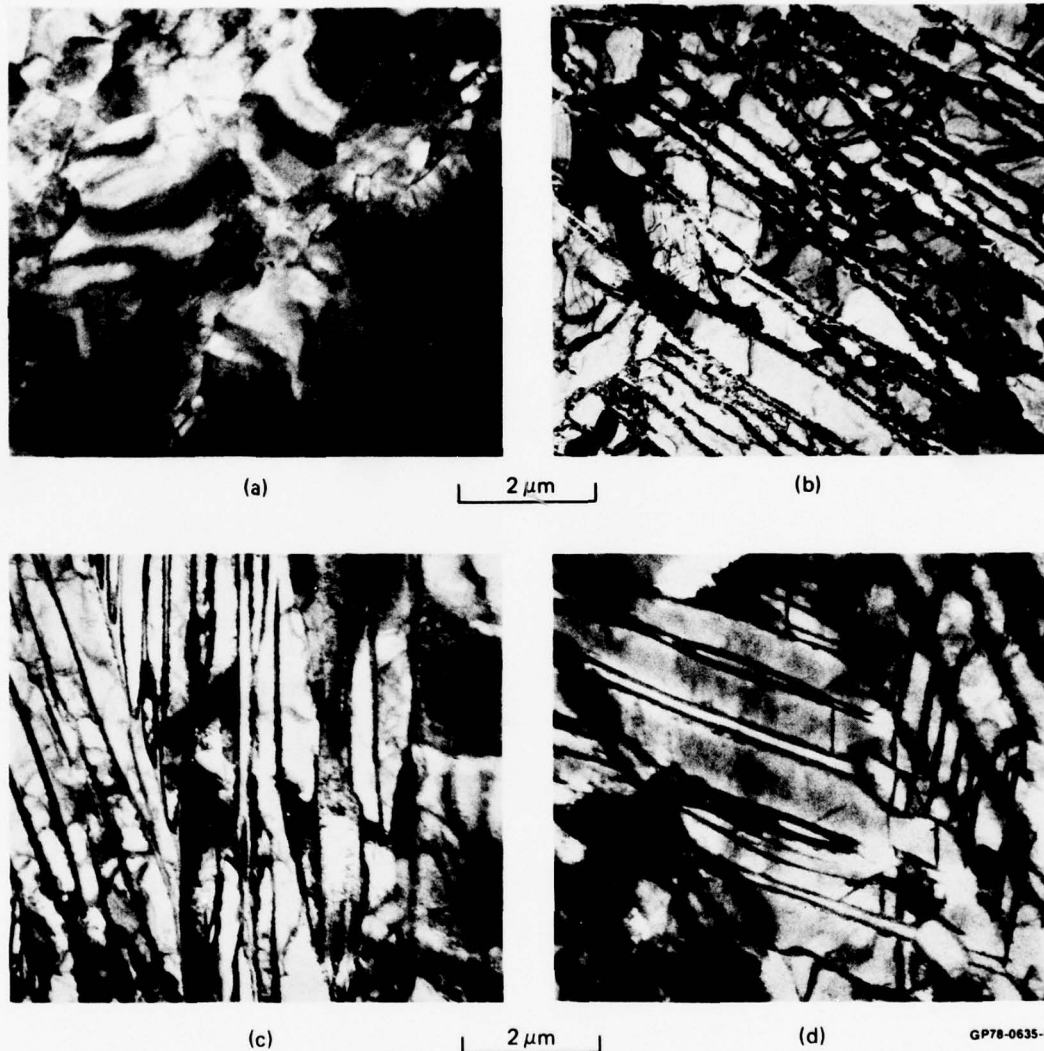


Figure 37. Effects of temperature and strain-rate on deformation substructure of Ti-6Al-4V specimens deformed in tension; (a) undeformed, (b) $T = 800^{\circ}\text{C}$, $\dot{\epsilon} = 0.01 \text{ s}^{-1}$, (c) $T = 800^{\circ}\text{C}$, $\dot{\epsilon} = 0.1 \text{ s}^{-1}$, and (d) $T = 856^{\circ}\text{C}$, $\dot{\epsilon} = 0.01 \text{ s}^{-1}$

8.2 High-Temperature Compression Test

Compression tests were performed on cylindrical specimens of 8.9-mm diam and 12-mm height using 60-mm diam stainless-steel compression rams. The sample and the flat faces of the rams were coated with several thin layers of Formkote T-50* to provide lubrication and inhibit oxidation. The specimens

* Tradename of E/M Lubricant, Inc., N. Hollywood, CA 91605.

were heated to the desired temperature in a three-zone, resistance-wound, split furnace and maintained at temperature for 10 minutes before compression was begun. Compression tests were conducted on mill-annealed and beta-annealed specimens at 700°, 800°, 850° and 900°C at a strain rate of 0.05 s⁻¹. The deformation-load and ram-displacement were recorded by an x-y plotter, and the true-stress/true-strain curves were constructed from the data.

The true-stress/true-strain curves at various temperatures for the mill-annealed and beta-annealed specimens are shown in Figures 38-43. The

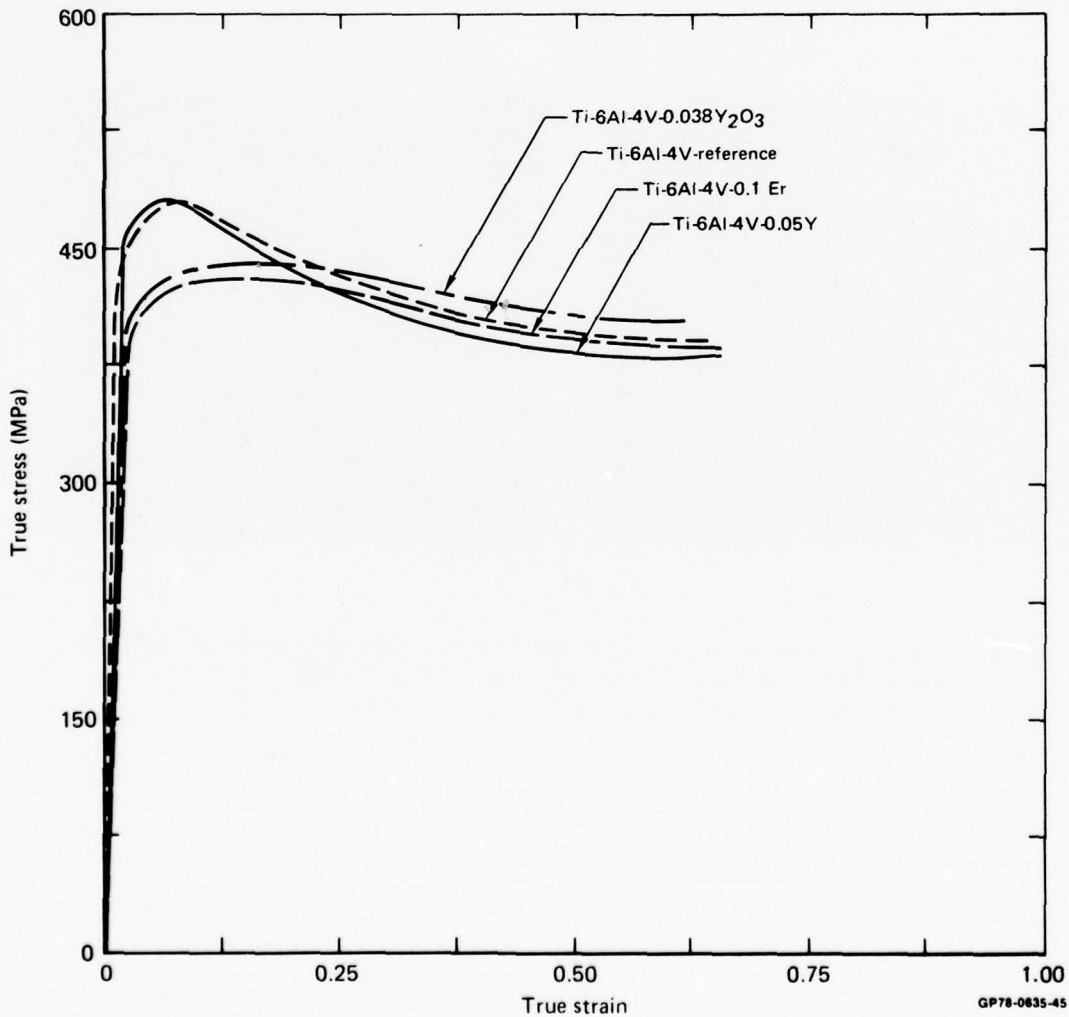


Figure 38. True-stress as a function of true-strain for beta-annealed Ti-6Al-4V-RE alloys deformed at 700°C at an initial strain rate of 0.05 s⁻¹

stress-strain curves are strongly influenced by initial microstructure and test temperature, but they are not significantly altered by the rare-earth additions because of the similarity of microstructures of the reference alloy and the Er- and Y-containing alloys in the heat-treated conditions. While the stress-strain curves of beta-annealed and mill-annealed specimens are similar at 800°C, the differences between the stress-strain characteristics of mill-annealed and β -annealed specimens are more pronounced at higher temperatures. The principal difference is the lower values of flow stress of mill-annealed specimens compared with those of beta-annealed specimens. A greater degree of initial softening is observed in beta-annealed specimens than in mill-annealed specimens. The flow stress increases with decreasing temperature.

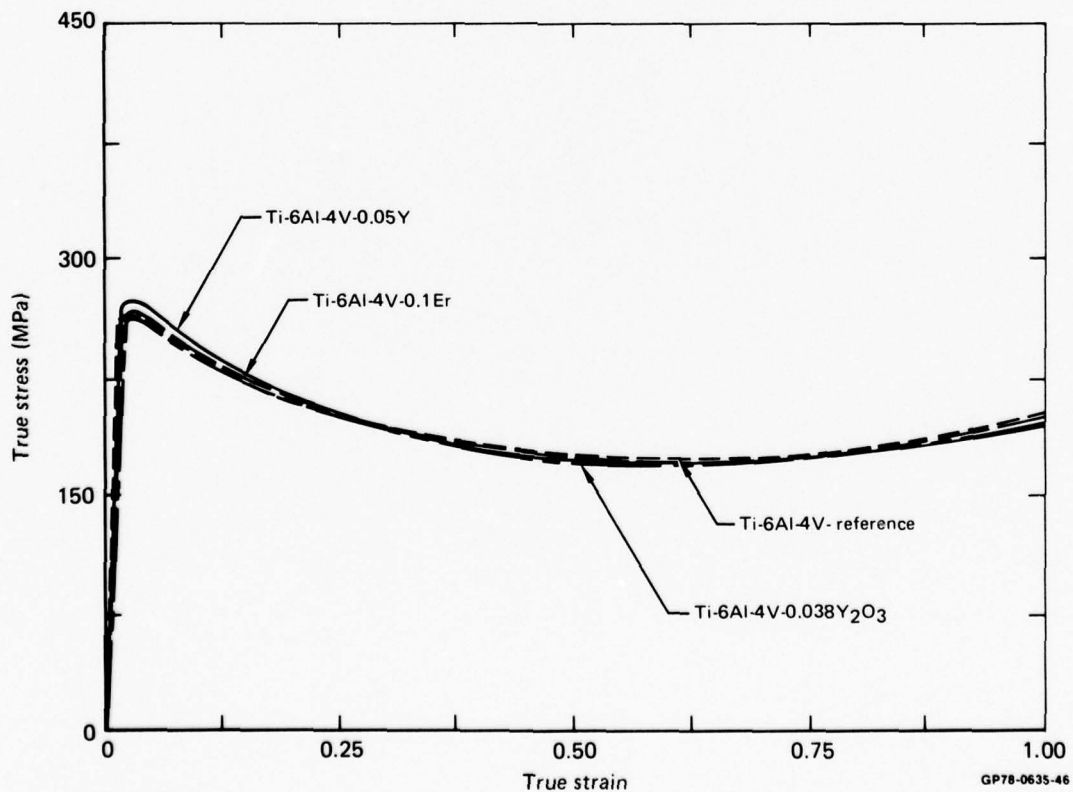


Figure 39. True-stress as a function of true-strain for beta-annealed Ti-6Al-4V-RE alloys deformed at 850°C at an initial strain-rate of 0.05 s⁻¹

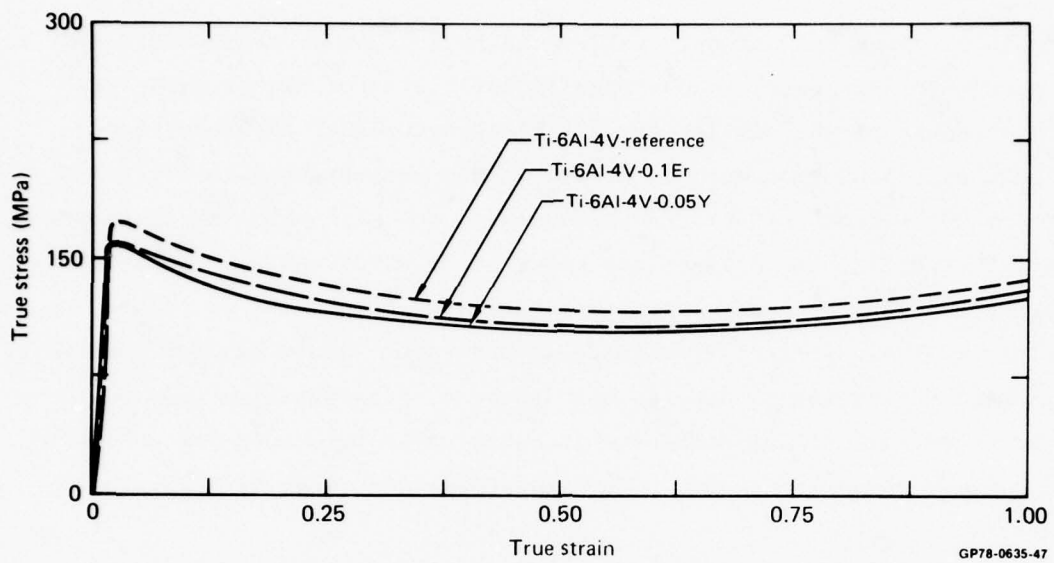


Figure 40. True-stress as a function of true-strain for beta-annealed Ti-6Al-4V-RE alloys deformed at 900°C at an initial strain rate of 0.05 s⁻¹

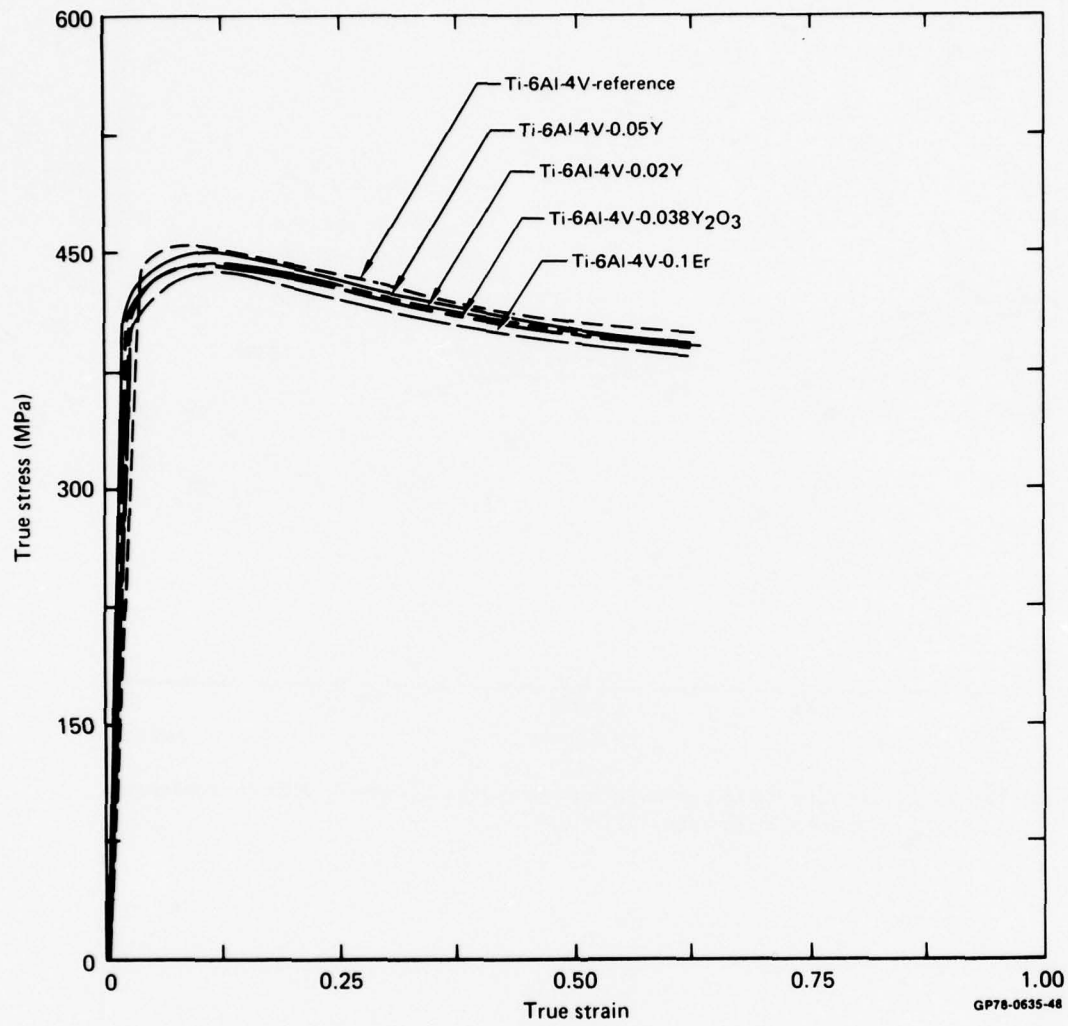


Figure 41. True-stress as a function of true-strain for mill-annealed Ti-6Al-4V-RE alloys deformed at 700°C at an initial strain rate of 0.05 s⁻¹

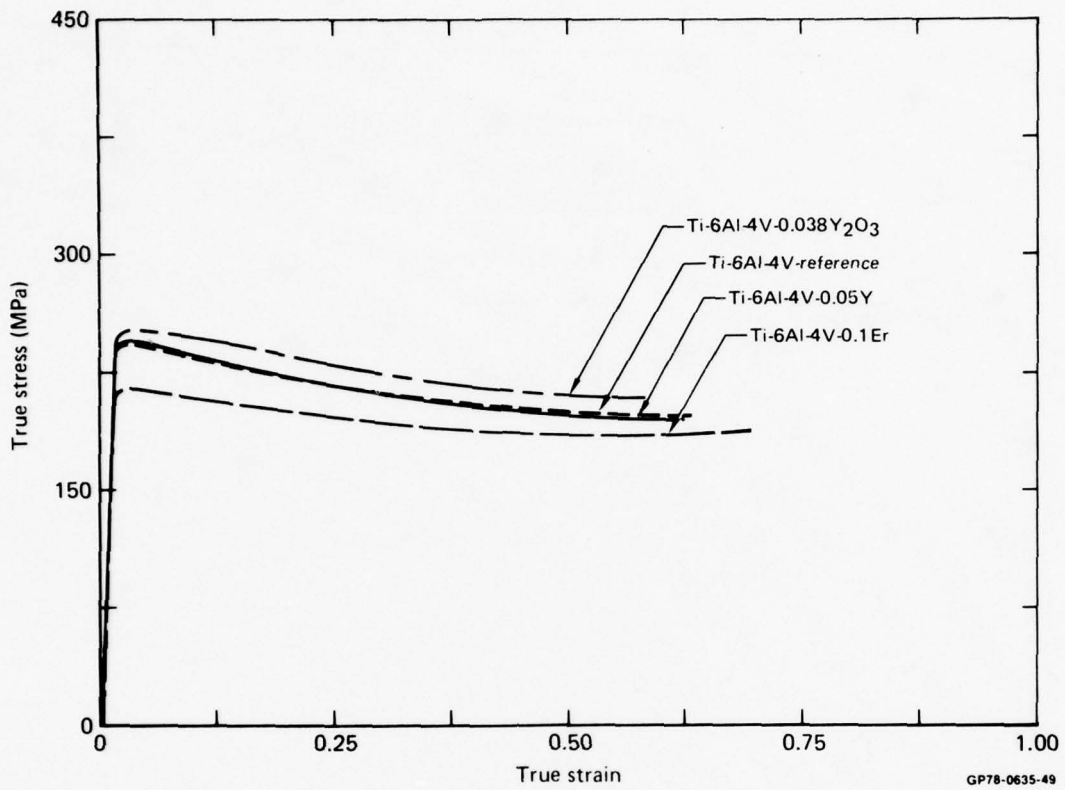


Figure 42. True-stress as a function of true-strain for mill-annealed Ti-6Al-4V-RE alloys deformed at 800°C at an initial strain rate of 0.05 s⁻¹

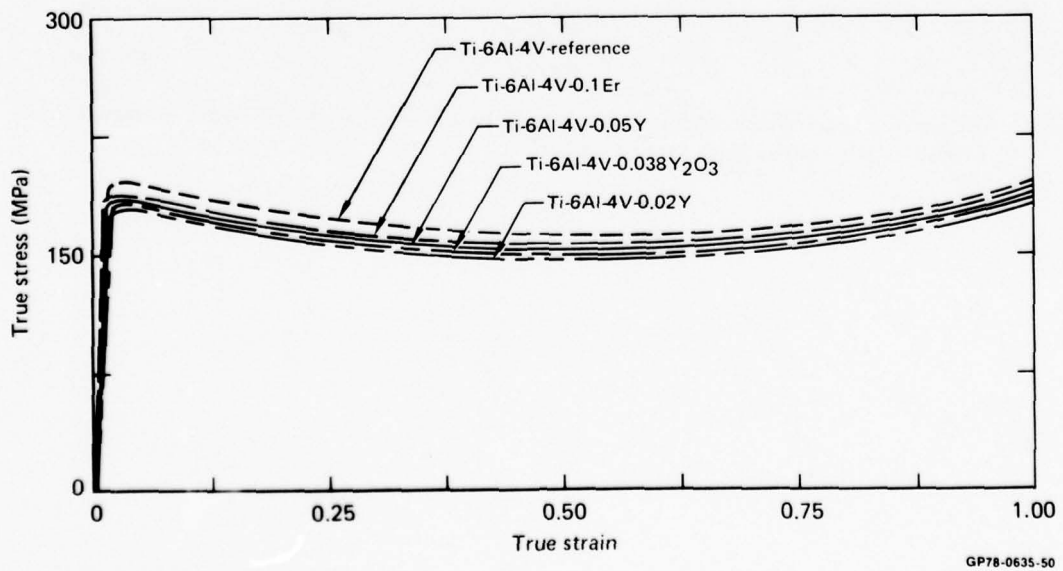


Figure 43. True-stress as a function of true-strain for mill-annealed Ti-6Al-4V-RE alloys deformed at 850°C at an initial strain rate of 0.05 s⁻¹

8.3 High-Temperature Deformation Substructures

The microstructures of beta-annealed specimens deformed at a strain rate of 0.05 s^{-1} at different temperatures are shown in Figures 44a-44d. At 700°C , extensive dislocation activity in the α phase, continuity of slip across the β phase, and absence of polygonization result in profuse shearing of the β phase. At 800°C and above, dynamic recovery occurs as evidenced by hexagonal networks of dislocations in the α phase and nearly-straight elongated α - β

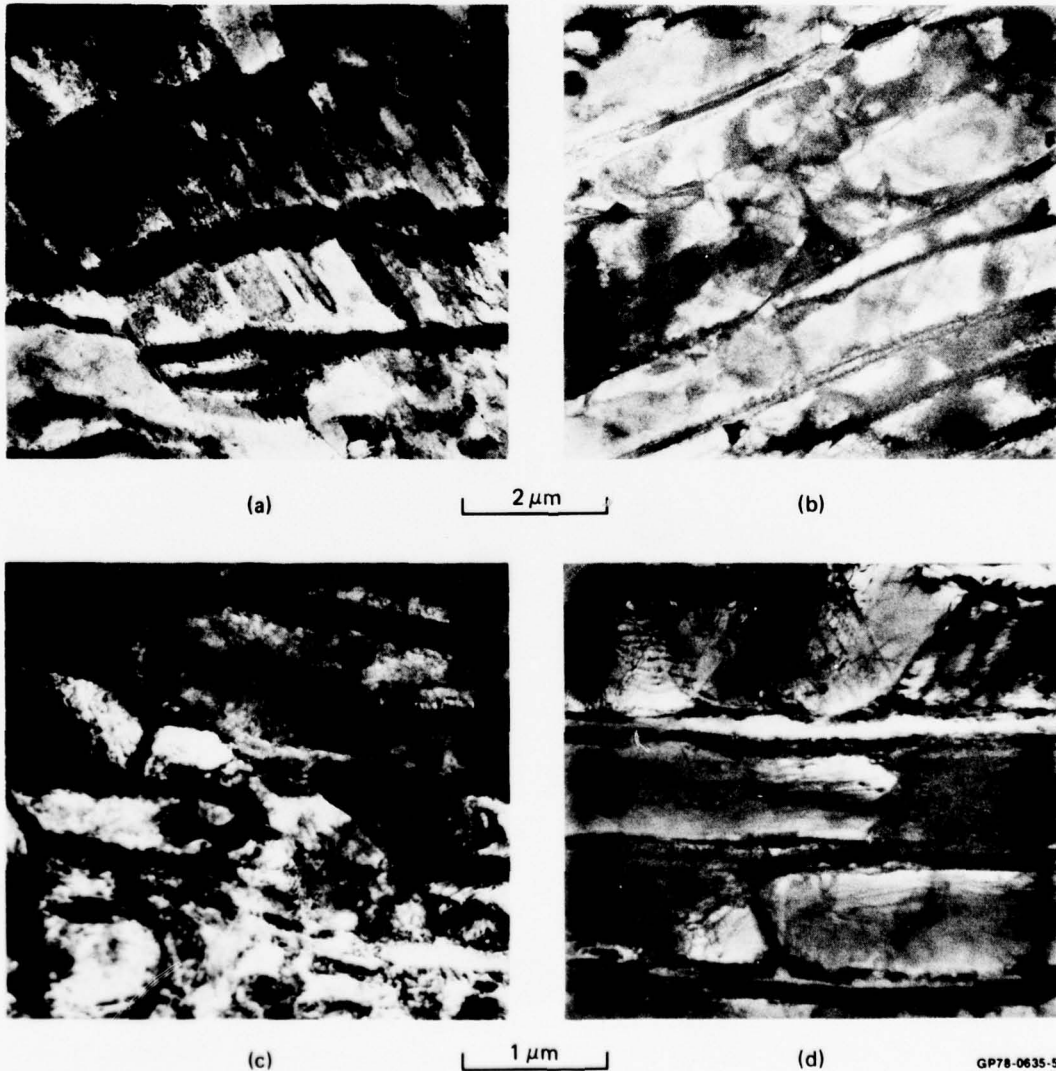
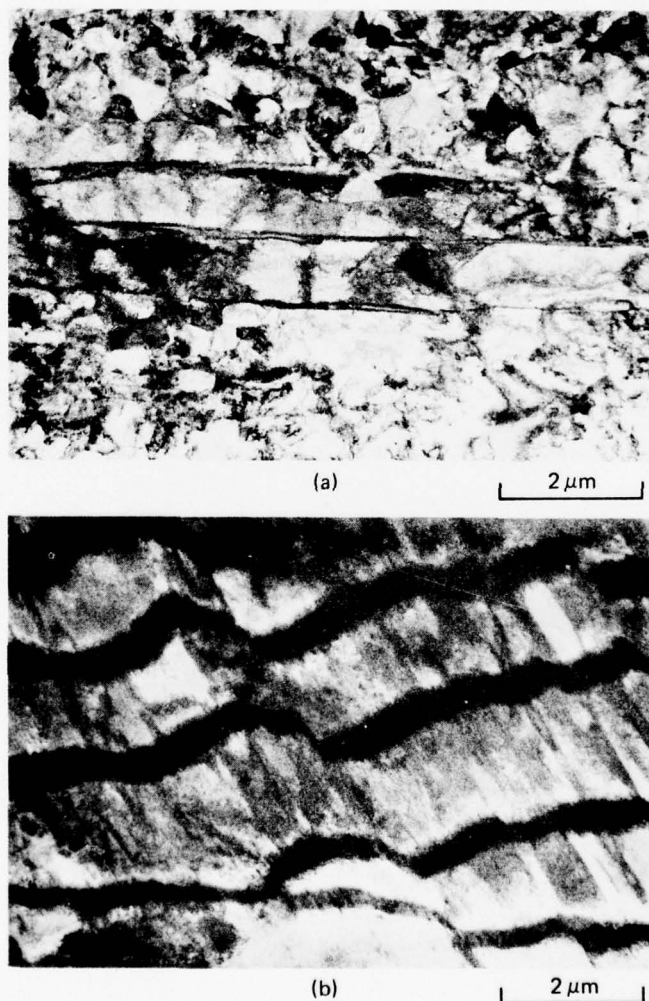


Figure 44. Effect of temperature on deformation substructures of beta-annealed Ti-6Al-4V specimens deformed in compression at an initial strain rate of 0.05 s^{-1} ; (a) 700°C , (b) 800°C , (c) 850°C , and (d) 900°C

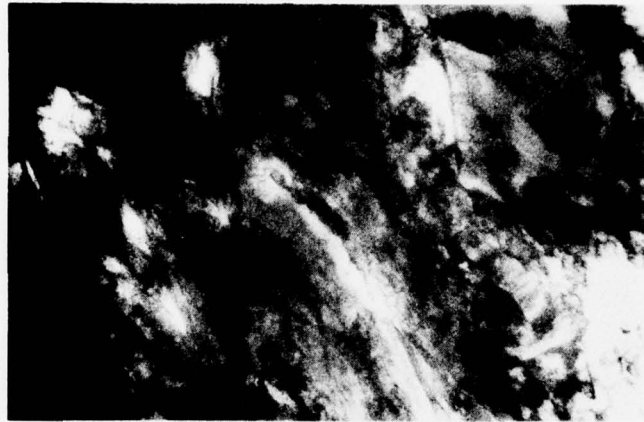
plates. The influence of strain rate on the deformation substructure of beta-annealed specimens deformed at 700°C is shown in Figure 45. At the slower strain rate of 0.001 s^{-1} , both dynamic recovery and recrystallization occur as evidenced by the absence of shearing of the β phase and the formation of small, equiaxed, alpha grains.



GP78-0635-52

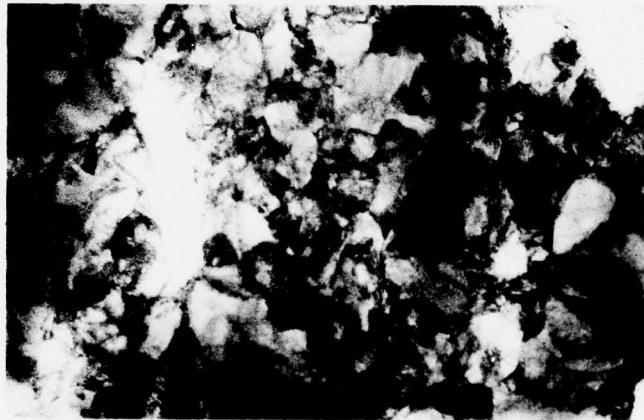
Figure 45. Effect of strain rate on deformation substructure of beta-annealed Ti-6Al-4V specimens deformed in compression at 700°C; (a) strain rate = 0.001 s^{-1} and (b) strain rate = 0.05 s^{-1}

The deformation substructures produced in mill-annealed specimens at 700°C, 800°C, and 850°C are shown in Figures 46a-46c. The deformation substructure produced at 700°C is characterized by a high dislocation density in the α phase without any dynamic recovery and recrystallization. At 800°C and 850°C, dynamic recovery and recrystallization occur continuously, resulting in fine equiaxed-alpha and grain-boundary beta (Figures 46b and 46c). Because at these temperatures, grain boundary sliding also contributes to deformation, the finer grain size in mill-annealed alloy results in reduced flow stresses.



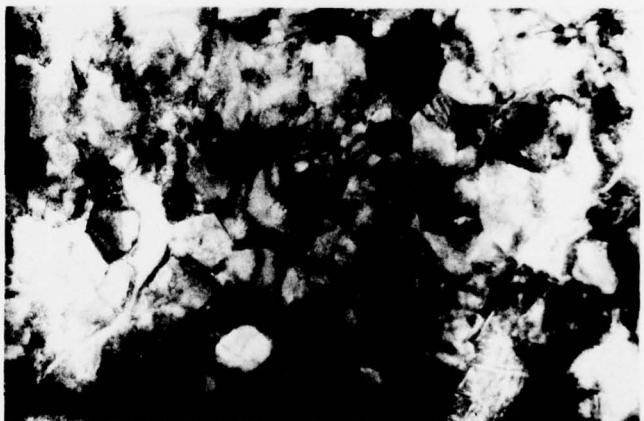
(a)

2 μm



(b)

2 μm



(c)

2 μm

GP78-0635-53

Figure 46. Effect of temperature on the deformation substructure of mill-annealed Ti-6Al-4V specimens deformed in compression at an initial strain rate of 0.05 s^{-1} ; (a) 700°C , (b) 800°C , and (c) 850°C

9. CONCLUSIONS

Conclusions based upon the study thus far of the Phase-II Ti-6Al-4V-RE alloys are qualified by the uncertainty of the rare-earth concentrations, which probably were about half the nominal values, and by the rare-earths not being uniformly dispersed. Additional chemical analyses and the study in progress of the Phase-III alloys should remove these ambiguities.

The addition of 0.02 wt% Y, 0.05 wt% Y, and 0.1 wt% Er to Ti-6Al-4V results in microstructural refinement similar to that observed in Phase I alloys. The grain-refinement effect of Y_2O_3 is similar to, but less pronounced than, that of metallic Y.

The room-temperature tensile properties of Ti-6Al-4V are not significantly altered by Er and Y additions. The tensile results are similar to those for Phase-I alloys.

Plane-strain and plane-stress fracture toughness of Ti-6Al-4V are not adversely affected by Er and Y additions.

The crystallographic texture developed during rolling of Ti-6Al-4V is unaffected by rare-earth additives. Annealing in the $\alpha+\beta$ field results in an increase in the sharpness of the near-transverse-basal texture components in the Y- and Y_2O_3 -containing alloys.

The uniform elongation of Ti-6Al-4V during high-temperature deformation is increased by Y and Er additions. The high-temperature compressive stress-strain characteristics of variously processed and heat-treated Ti-6Al-4V are not altered by Y and Er additions.

REFERENCES

1. C. R. Whitsett, S. M. L. Sastry, J. E. O'Neal, and R. J. Lederich, Influence of Rare-Earth Additions on Properties of Titanium Alloys: Microstructures and Room-Temperature Tensile Properties of Ti-6Al-4V with Yttrium, Erbium, and Mischmetal Additions, Technical Report for period 1 April 1976-31 March 1977 for ONR contract N00014-76-C-0626, Report MDC Q0627 (31 May 1978).
2. M. J. Buczek, G. S. Jall, S. R. Seagle, and H. B. Bomberger, Grain Refinement of Titanium Alloys, AFML-TR-74-255, November 1974.
3. B. B. Rath, R. J. Lederich, and J. E. O'Neal, Recrystallization and Grain Growth in Ti-Rare Earth Alloys, ASM-AIME Materials Science Symposium, Cincinnati, OH, November 1975.
4. B. B. Rath, R. J. Lederich, and J. E. O'Neal, The Effects of Rare-Earth Additions on the Grain Refinement of Ti, in Grain Boundaries in Engineering Materials, ed. by J. L. Walter, J. H. Westbrook, and D. A. Woodford (Claitors Publ. Div., Baton Rouge, LA, 1975), p. 39.
5. B. B. Rath, J. E. O'Neal, and R. J. Lederich, Grain Refinement in Ti-Er Alloys, in Proc. Electron Microscopy Soc. Am., ed. by C. J. Arceneaux, (Claitors Publ. Div., Baton Rouge, LA, 1974), p. 522.
6. R. G. Forman, Effect of Plastic Deformation on the Strain Energy Release Rate in a Centrally Notched Plate Subjected to Uniaxial Tension, Trans. ASME, J. Basic Engineering 88, 82 (1966).

APPENDIX A: ROOM-TEMPERATURE TENSILE PROPERTIES AND FRACTURE
TOUGHNESS OF PHASE-II Ti-6Al-4V-RE ALLOYS

Tables A1-A6 list the room-temperature tensile properties of the Ti-6Al-4V reference, Ti-6Al-4V-0.1Er, Ti-6Al-4V-0.02Y, Ti-6Al-4V-0.05Y, and Ti-6Al-4V-0.038Y₂O₃ alloys prepared for the Phase-II study. Each of Tables A1-A6 is for a different heat treatment. Tables A7-A9 list the fracture toughness values determined by three-point slow-bend testing of fatigue-precracked Charpy V-notched specimens subjected to three different heat treatments. Table A10 lists the plane-stress fracture-toughness values for the alloys.

TABLE A1. ROOM-TEMPERATURE TENSILE PROPERTIES OF PHASE-II Ti-6Al-4V-RE ALLOYS IN THE LONGITUDINAL (L) AND TRANSVERSE (T) DIRECTIONS; HOT-ROLLED AND UNANNEALED, AS RECEIVED

Alloy composition	Processing condition	Yield stress at 0.2% offset (MPa)		Ultimate tensile stress (MPa)		Uniform elongation (%)		Total elongation (%)	
		L	T	L	T	L	T	L	T
Ti-6Al-4V	A	930	998	960	1028	5.6	3.8	11.6	10.3
	B	—	923	—	975	—	2.9	—	11.1
Ti-6Al-4V-0.02Y	A	998	910	1028	975	4.8	4.5	11.8	12.6
	B	870	960	945	1005	5.5	4.5	13.5	13.5
Ti-6Al-4V-0.05Y	A	938	1005	975	1020	4.8	4.0	14.5	11.8
	B	900	923	960	1012	5.3	4.1	13.7	12.7
Ti-6Al-4V-0.10Er	A	900	960	930	1013	6.3	3.8	14.3	12.6
	B	870	930	938	997	5.5	4.0	13.0	13.4
Ti-6Al-4V-0.038Y ₂ O ₃	A	953	990	983	1043	5.8	5.1	15.8	13.2
	B	870	953	908	998	5.1	3.8	12.2	12.8

Processing condition: A = continuously rolled from 26 mm to 13 mm thickness from 940°C
B = continuously rolled from 26 mm to 13 mm thickness from 1025°C

GP78-0635-5

TABLE A2. ROOM-TEMPERATURE TENSILE PROPERTIES OF PHASE-II Ti-6Al-4V-RE ALLOYS IN THE LONGITUDINAL (L) AND TRANSVERSE (T) DIRECTIONS; RECRYSTALLIZATION ANNEALED

Alloy composition	Processing condition	Yield stress at 0.2% offset (MPa)		Ultimate tensile stress (MPa)		Uniform elongation (%)		Total elongation (%)	
		L	T	L	T	L	T	L	T
Ti-6Al-4V	A	—	848	—	894	—	8.2	—	16.3
	B	765	758	855	848	7.3	4.0	16.2	10.8
Ti-6Al-4V-0.02Y	A	780	863	855	938	5.7	8.0	12.0	16.2
	B	780	780	855	863	6.2	4.3	16.0	16.0
Ti-6Al-4V-0.05Y	A	870	855	938	930	7.2	7.2	15.4	14.1
	B	833	745	915	878	7.2	4.5	16.2	15.8
Ti-6Al-4V-0.10Er	A	758	862	833	910	6.0	7.2	15.3	14.8
	B	788	780	870	870	7.2	4.2	16.3	14.9
Ti-6Al-4V-0.038Y ₂ O ₃	A	855	870	923	953	6.9	8.1	16.2	16.2
	B	795	780	880	870	5.9	4.0	16.1	14.4

Processing condition: A = continuously rolled from 26 mm to 13 mm thickness from 940°C
 B = continuously rolled from 26 mm to 13 mm thickness from 1025°C

GP78-0635-6

TABLE A3. ROOM-TEMPERATURE TENSILE PROPERTIES OF PHASE-II Ti-6Al-4V-RE ALLOYS IN THE LONGITUDINAL (L) AND TRANSVERSE (T) DIRECTIONS; BETA ANNEALED

Alloy composition	Processing condition	Yield stress at 0.2% offset (MPa)		Ultimate tensile stress (MPa)		Uniform elongation (%)		Total elongation (%)	
		L	T	L	T	L	T	L	T
Ti-6Al-4V	A	870	855	920	923	3.3	3.6	8.5	7.7
	B	840	863	923	915	3.9	3.1	10.1	9.2
Ti-6Al-4V-0.02Y	A	877	848	953	930	5.3	3.9	12.0	8.8
	B	840	848	923	930	5.1	4.5	12.6	13.3
Ti-6Al-4V-0.05Y	A	863	855	953	947	4.4	4.9	11.5	11.0
	B	840	863	930	953	5.4	5.4	14.5	13.9
Ti-6Al-4V-0.10Er	A	840	—	915	—	4.8	—	12.8	—
	B	848	863	938	945	5.3	5.1	13.5	14.2
Ti-6Al-4V-0.038Y ₂ O ₃	A	885	855	960	945	5.4	4.3	11.0	9.3
	B	877	885	945	945	4.9	3.8	14.0	11.2

Processing condition: A = continuously rolled from 26 mm to 13 mm thickness from 940°C
 B = continuously rolled from 26 mm to 13 mm thickness from 1025°C

GP78-0635-7

TABLE A4. ROOM-TEMPERATURE TENSILE PROPERTIES OF PHASE-II Ti-6Al-4V-RE ALLOYS IN THE LONGITUDINAL (L) AND TRANSVERSE (T) DIRECTIONS; SOLUTION-TREAT-AND-AGED

Alloy composition	Processing condition	Yield stress at 0.2% offset (MPa)		Ultimate tensile stress (MPa)		Uniform elongation (%)		Total elongation (%)	
		L	T	L	T	L	T	L	T
Ti-6Al-4V	A	1020	1072	1110	1178	2.4	1.8	5.0	3.8
	B	1080	—	1163	—	2.4	—	4.6	—
Ti-6Al-4V-0.02Y	A	1230	—	1298	—	—	1.8	—	4.5
	B	1103	1080	1178	1170	2.8	2.4	7.2	6.8
Ti-6Al-4V-0.05Y	A	1125	—	1200	—	—	1.7	—	4.1
	B	1110	1013	1205	1133	3.8	2.9	7.9	7.1
Ti-6Al-4V-0.10Er	A	—	—	—	—	—	—	—	—
	B	—	—	—	—	—	—	—	—
Ti-6Al-4V-0.038Y ₂ O ₃	A	1103	—	1193	—	2.7	—	5.6	—
	B	1110	1133	1193	1200	2.8	2.4	6.6	6.1

Processing condition: A = continuously rolled from 26 mm to 13 mm thickness from 940°C
 B = continuously rolled from 26 mm to 13 mm thickness from 1025°C

GP78-0635-8

TABLE A5. ROOM-TEMPERATURE TENSILE PROPERTIES OF PHASE-II Ti-6Al-4V-RE ALLOYS IN THE LONGITUDINAL (L) AND TRANSVERSE (T) DIRECTIONS; SOLUTION-TREAT-AND-OVERAGED

Alloy composition	Processing condition	Yield stress at 0.2% offset (MPa)		Ultimate tensile stress (MPa)		Uniform elongation (%)		Total elongation (%)	
		L	T	L	T	L	T	L	T
Ti-6Al-4V	A	—	1020	—	1088	—	2.7	—	5.8
	B	990	975	1057	1050	3.7	3.1	7.6	5.7
Ti-6Al-4V-0.02Y	A	983	1028	1073	1080	3.8	2.9	7.8	6.9
	B	998	998	1080	1073	3.5	3.2	10.2	9.0
Ti-6Al-4V-0.05Y	A	1013	990	1088	1073	3.8	2.8	10.0	7.0
	B	998	1028	1080	1088	3.8	3.6	10.7	9.5
Ti-6Al-4V-0.10Er	A	983	990	1050	1065	3.0	2.8	9.8	6.7
	B	990	975	1073	1057	3.0	3.8	8.0	10.3
Ti-6Al-4V-0.038Y ₂ O ₃	A	998	998	1070	1080	3.2	3.0	6.8	6.2
	B	1020	998	1088	1080	4.2	3.5	9.9	7.8

Processing condition: A = continuously rolled from 26 mm to 13 mm thickness from 940°C
 B = continuously rolled from 26 mm to 13 mm thickness from 1025°C

GP78-0635-9

TABLE A6. ROOM-TEMPERATURE TENSILE PROPERTIES OF PHASE-II Ti-6Al-4V-RE ALLOYS IN THE LONGITUDINAL (L) AND TRANSVERSE (T) DIRECTIONS: α - β ANNEALED AND AGED

Alloy composition	Processing condition	Yield stress at 0.2% offset (MPa)		Ultimate tensile stress (MPa)		Uniform elongation (%)		Total elongation (%)	
		L	T	L	T	L	T	L	T
Ti-6Al-4V	A	825	878	923	945	5.6	7.3	14.2	16.3
	B	795	848	900	923	6.8	5.6	16.1	13.8
Ti-6Al-4V-0.02Y	A	848	885	945	945	6.6	4.9	14.8	12.1
	B	810	855	915	923	6.1	5.2	14.2	12.2
Ti-6Al-4V-0.05Y	A	885	893	975	960	7.7	5.6	16.5	14.6
	B	825	885	923	945	5.8	5.1	15.4	10.9
Ti-6Al-4V-0.10Er	A	840	848	938	923	6.7	4.7	14.4	12.7
	B	803	870	893	945	6.2	6.6	15.1	14.6
Ti-6Al-4V-0.038Y ₂ O ₃	A	893	893	975	960	8.3	5.4	16.2	11.4
	B	775	885	900	907	4.9	4.1	13.6	11.9

Processing condition: A = continuously rolled from 26 mm to 13 mm thickness from 940°C
 B = continuously rolled from 26 mm to 13 mm thickness from 1025°C

GP78-0635-10

TABLE A7. FRACTURE TOUGHNESS VALUES (K_Q) DETERMINED FROM SLOW-BEND, PRECRACKED, CHARPY SAMPLES OF RECRYSTALLIZATION-ANNEALED PHASE-II Ti-6Al-4V-RE ALLOYS

Alloy composition	Rolling schedule	K _Q [MPa \sqrt{m} (ksi $\sqrt{in.}$)]		
		T-L	L-T	T-S
Ti-6Al-4V	A	84.7 (77)	92.4 (84)	115.5 (105)
	B	127.6 (116)	94.6 (86)	116.6 (106)
Ti-6Al-4V-0.02Y	A	85.8 (78)	81.4 (74)	100.1 (91)
	B	86.9 (79)	95.7 (87)	86.9 (79)
Ti-6Al-4V-0.05Y	A	80.3 (73)	—	96.8 (88)
	B	63.8 (58)	89.1 (81)	77.0 (70)
Ti-6Al-4V-0.10Er	A	75.9 (69)	83.6 (76)	78.1 (71)
	B	91.3 (83)	101.2 (92)	115.5 (105)
Ti-6Al-4V-0.038Y ₂ O ₃	A	82.5 (75)	90.2 (82)	141.9 (129)
	B	—	102.3 (93)	92.4 (84)

Processing condition: A = continuously rolled from 26 mm to 13 mm thickness from 940°C
 B = continuously rolled from 26 mm to 13 mm thickness from 1025°C

GP78-0635-11

TABLE A8. FRACTURE TOUGHNESS VALUES (K_Q) DETERMINED FROM SLOW-BEND, PRECRACKED, CHARPY SAMPLES OF BETA-ANNEALED PHASE-II Ti-6Al-4V-RE ALLOYS

Alloy composition	Rolling schedule	K_Q [MPa \sqrt{m} (ksi $\sqrt{in.}$)]		
		T-L	L-T	T-S
Ti-6Al-4V	A	85.8 (78)	96.8 (88)	90.2 (82)
	B	94.6 (86)	85.8 (78)	89.1 (81)
Ti-6Al-4V-0.02Y	A	71.5 (65)	81.4 (74)	70.4 (64)
	B	69.3 (63)	74.8 (68)	72.6 (66)
Ti-6Al-4V-0.05Y	A	58.3 (53)	75.9 (69)	59.4 (54)
	B	58.3 (53)	72.6 (66)	62.7 (57)
Ti-6Al-4V-0.10Er	A	63.8 (58)	72.6 (66)	72.6 (66)
	B	72.6 (66)	80.3 (73)	68.2 (62)
Ti-6Al-4V-0.038Y ₂ O ₃	A	70.4 (64)	81.4 (74)	75.9 (69)
	B	73.7 (67)	77.0 (70)	75.9 (69)

Processing condition: A = continuously rolled from 26 mm to 13 mm thickness from 940°C
B = continuously rolled from 26 mm to 13 mm thickness from 1025°C

GP78-0635-12

TABLE A9. FRACTURE TOUGHNESS VALUES (K_Q) DETERMINED FROM SLOW-BEND, PRECRACKED, CHARPY SAMPLES OF SOLUTION-TREAT-AND-OVERAGED PHASE-II Ti-6Al-4V-RE ALLOYS

Alloy composition	Rolling schedule	K_Q [MPa \sqrt{m} (ksi $\sqrt{in.}$)]		
		T-L	L-T	T-S
Ti-6Al-4V	A	N.D.	46.2 (42)	50.6 (46)
	B	52.8 (48)	—	51.7 (47)
Ti-6Al-4V-0.02Y	A	42.9 (39)	46.2 (42)	45.1 (41)
	B	33.0 (30)	41.8 (38)	40.7 (37)
Ti-6Al-4V-0.05Y	A	37.4 (34)	33.0 (30)	40.7 (37)
	B	40.7 (37)	49.5 (45)	35.2 (32)
Ti-6Al-4V-0.10Er	A	44.0 (40)	N.D.	42.9 (39)
	B	42.9 (39)	45.1 (41)	44.0 (40)
Ti-6Al-4V-0.038Y ₂ O ₃	A	44.0 (40)	38.5 (35)	—
	B	33.0 (30)	45.1 (41)	45.1 (41)

Processing condition: A = continuously rolled from 26 mm to 13 mm thickness from 940°C
B = continuously rolled from 26 mm to 13 mm thickness from 1025°C

GP78-0635-13

TABLE A10. PLANE-STRESS FRACTURE TOUGHNESS VALUES DETERMINED FROM CENTER-CRACKED TENSION SPECIMENS OF PHASE-II Ti-6Al-4V-RE ALLOYS

Alloy	Alloy composition	Rolling schedule	Fracture toughness K_Q [MPa \sqrt{m} (ksi $\sqrt{in.}$)]		
			Beta annealed	Recrystallization annealed	Solution-treat-and-aged
31	Ti-6Al-4V	A	132 (120)	130 (118)	143 (130)
		B	140 (127)	—	151 (137)
33	Ti-6Al-4V-0.02Y	A	154 (140)	123 (112)	136 (124)
		B	153 (139)	—	121 (110)
34	Ti-6Al-4V-0.05Y	A	152 (138)	123 (112)	—
		B	158 (144)	—	139 (126)
32	Ti-6Al-4V-0.10Er	A	165 (150)	130 (118)	134 (122)
		B	154 (140)	—	136 (124)
36	Ti-6Al-4V-0.038Y ₂ O ₃	A	161 (146)	134 (122)	129 (117)
		B	143 (130)	—	150 (136)

Processing condition: A = continuously rolled from 26 mm to 13 mm thickness from 940°C
 B = continuously rolled from 26 mm to 13 mm thickness from 1025°C

GP78-0635-14

DISTRIBUTION

	Copies		Copies
Defense Documentation Center Cameron Station Alexandria, VA 22314	12	Naval Construction Battalion Civil Engineering Laboratory Port Hueneme, CA 93043 Attn: Materials Division	1
Office of Naval Research Department of the Navy 800 N. Quincy Street Arlington, VA 22217 Attn: Code 471 Code 102 Code 470	1 1 1	Naval Electronics Laboratory San Diego, CA 92152 Attn: Electron Materials Sciences Division	1
Commanding Officer Office of Naval Research Branch Office Building 114, Section D 666 Summer Street Boston, MA 02210	1	Naval Missile Center Materials Consultant Code 3312-1 Point Mugu, CA 92041	1
Commanding Officer Office of Naval Research Branch Office 536 South Clark Street Chicago, IL 60605	1	Commanding Officer Naval Surface Weapons Center White Oak Laboratory Silver Spring, MD 20910 Attn: Library	1
Office of Naval Research San Francisco Area Office 760 Market Street, Room 447 San Francisco, CA 94102	1	David W. Taylor Naval Ship R&D Center Materials Department Annapolis, MD 21402	1
Naval Research Laboratory Washington, D. C. 20375 Attn: Code 6000 Code 6100 Code 6300 Code 6400 Code 2627	1 1 1 1 1	Naval Undersea Center San Diego, CA 92132 Attn: Library	1
Naval Air Development Center Code 302 Warminster, PA 18964 Attn: Mr. F. S. Williams	1	Naval Underwater System Center Newport, RI 02840 Attn: Library	1
Naval Air Propulsion Test Center Trenton, N. J. 08628 Attn: Library	1	Naval Weapons Center China Lake, CA 93555 Attn: Library	1
		Naval Postgraduate School Monterey, CA 93940 Attn: Mechanical Engineering Department	1
		Naval Air Systems Command Washington, D. C. 20360 Attn: Code 52031 Code 52032	1 1

	Copies		Copies
Naval Sea System Command Washington, D. C. 20362 Attn: Code 035	1	NASA Headquarters Washington, D. C. 20546 Attn: Code RRM	1
Naval Facilities Engineering Command Alexandria, VA 22331 Attn: Code 03	1	NASA Lewis Research Center 21000 Brookpark Road Cleveland, OH 44135 Attn: Library	1
Scientific Advisor Commandant of the Marine Corps Washington, D. C. 20380 Attn: Code AX	1	National Bureau of Standards Washington, D. C. 20234 Attn: Metallurgy Division Inorganic Materials Div.	1 1
Naval Ship Engineering Center Department of the Navy Washington, D. C. 20360 Attn: Code 6101	1	Director Applied Physics Laboratory University of Washington 1013 Northeast Forthieth Street Seattle, WA 98105	1
Army Research Office P.O. Box 12211 Triangle Park, N. C. 27709 Attn: Metallurgy & Ceramics Program	1	Defense Metals and Ceramics Information Center Battelle Memorial Institute 505 King Avenue Columbus, OH 43201	1
Army Materials and Mechanics Research Center Watertown, MA 02172 Attn: Research Programs Office	1	Metals and Ceramics Division Oak Ridge National Laboratory P.O. Box X Oak Ridge, TN 37380	1
Air Force Office of Scientific Research Bldg. 410 Bolling Air Force Base Washington, D. C. 20332 Attn: Chemical Science Directorate	1	Los Alamos Scientific Laboratory P.O. Box 1663 Los Alamos, NM 87544 Attn: Report Librarian	1
	1	Argonne National Laboratory Metallurgy Division P.O. Box 229 Lemont, IL 60439	1
Air Force Materials Laboratory Wright-Patterson AFB Dayton, OH 45433	1	Brookhaven National Laboratory Technical Information Division Upton, Long Island New York 11973 Attn: Research Library	1
Library Building 50, Rm 134 Lawrence Radiation Laboratory Berkeley, CA	1	Office of Naval Research Branch Office 1030 East Green Street Pasadena, CA 91106	1

	Copies		Copies
Professor G. S. Ansell Rensselaer Polytechnic Institute Dept. of Metallurgical Engineering Troy, New York 12181	1	Professor Thomas W. Eagar Massachusetts Institute of Technology Department of Materials Science and Engineering Cambridge, MA 02139	1
Professor H. K. Birnbaum University of Illinois Department of Metallurgy Urbana, IL 61801	1	Professor B. C. Giessen Northeastern University Department of Chemistry Boston, MA 02115	1
Mr. H. B. Bomberger Director Metallurgy and Research RMI Company Niles, OH 44446	1	Dr. G. T. Hahn Battelle Memorial Institute Department of Metallurgy 505 King Avenue Columbus, OH 43201	1
Dr. E. M. Breinan United Aircraft Corporation United Aircraft Res. Laboratories East Hartford, CT 06108	1	Professor D. G. Howden Ohio State University Dept. of Welding Engineering 190 West 19th Avenue Columbus, OH 43210	1
Professor H. D. Brody University of Pittsburgh School of Engineering Pittsburgh, PA 14213	1	Dr. C. S. Kortovich TRW, Inc. 23555 Euclid Avenue Cleveland, OH 44117	1
Mr. P. J. Cacciatore General Dynamics Electric Boat Division Eastern Point Road Groton, CT 06340	1	Professor D. A. Koss Michigan Technological University College of Engineering Houghton, MI 49931	1
Mr. Larry Clark Building 653/Room 325 Air Force Materials Laboratory Wright-Patterson AFB Dayton, OH 45433	1	Professor A. Lawley Drexel University Dept. of Metallurgical Engineering Philadelphia, PA 19104	1
Professor J. B. Cohen Northwestern University Dept. of Material Sciences Evanston, IL 60201	1	Professor Harris Marcus The University of Texas at Austin College of Engineering Austin, TX 78712	1
Professor M. Cohen Massachusetts Institute of Technology Department of Metallurgy Cambridge, MA 02139	1	Dr. H. Margolin Polytechnic Institute of New York 333 Jay Street Brooklyn, New York 11201	1

	Copies		Copies
Professor K. Masubuchi Massachusetts Institute of Technology Department of Ocean Engineering Cambridge, MA 02139	1	Professor J. Shyne Stanford University Materials Sciences Division Stanford, CA 94300	1
Dr. H. I. McHenry National Bureau of Standards Institute for Basic Standards Boulder, CO 80302	1	Dr. R. P. Simpson Westinghouse Electric Corporation Research & Development Center Pittsburgh, PA 15235	1
Professor J. W. Morris, Jr. University of California College of Engineering Berkeley, CA 94720	1	Dr. E. A. Starke, Jr. Georgia Institute of Technology School of Chemical Engineering Atlanta, GA 30332	1
Professor Ono University of California Materials Department Los Angeles, CA 90024	1	Professor David Turnbull Harvard University Division of Engineering and Applied Physics Cambridge, MA 02139	1
Dr. Neil E. Paton Rockwell International Science Center 1049 Camino Dos Rios P.O. Box 1085 Thousand Oaks, CA 91360	1	Dr. F. E. Wawner University of Virginia School of Engineering and Applied Science Charlottesville, VA 22901	1
Professor M. E. Paulaitis Department of Chemical Engineering University of Delaware Newark, Delaware 19711	1	Dr. C. R. Whitsett McDonnell Douglas Research Labs. McDonnell Douglas Corporation St. Louis, MO 63166	1
Mr. A. Pollack Naval Ships Research & Development Center Annapolis, MD 21402	1	Dr. J. C. Williams Carnegie-Mellon University Department of Metallurgy and Materials Sciences Schenley Park Pittsburgh, PA 15213	1
Dr. Karl M. Prewé United Technologies Laboratories United Technologies Corporation East Hartford, CT 06108	1	Professor H. G. F. Wilsdorf University of Virginia Charlottesville, VA 22903	1
Professor W. F. Savage Rensselaer Polytechnic Institute School of Engineering Troy, New York 12181	1	Dr. M. A. Wright University of Tennessee Space Institute Tullahoma, TN 37388	1
Professor O. D. Sherby Stanford University Materials Sciences Division Stanford, CA 94300	1		